

Dipolar ordering transitions in many-body quantum optics: Analytical diagrammatic approach to equilibrium quantum spins

Benedikt Schneider ^{1,2}, Ruben Burkard ³, Beatriz Olmos ³, Igor Lesanovsky ^{4,5} and Björn Sbierski ³

¹*Department of Physics and Arnold Sommerfeld Center for Theoretical Physics,*

Ludwig-Maximilians-Universität München, Theresienstr. 37, 80333 Munich, Germany

²*Munich Center for Quantum Science and Technology (MCQST), 80799 Munich, Germany*

³*Institut für Theoretische Physik, Universität Tübingen, Auf der Morgenstelle 14, 72076 Tübingen, Germany*

⁴*Institut für Theoretische Physik and Center for Integrated Quantum Science and Technology,*

Universität Tübingen, Auf der Morgenstelle 14, 72076 Tübingen, Germany

⁵*School of Physics and Astronomy and Centre for the Mathematics and Theoretical Physics of Quantum Non-Equilibrium Systems, The University of Nottingham, Nottingham NG7 2RD, United Kingdom*



(Received 16 August 2024; revised 20 October 2024; accepted 12 November 2024; published 2 December 2024)

Quantum spin models with a large number of interaction partners per spin are frequently used to describe modern many-body quantum optical systems such as arrays of Rydberg atoms, atom-cavity systems, or trapped ion crystals. For theoretical analysis the mean-field (MF) ansatz is routinely applied. However, besides special cases of all-to-all or strong long-range interactions, the MF ansatz provides only approximate results. Here we present a systematic correction to MF theory based on diagrammatic perturbation theory for quantum spin correlators in thermal equilibrium. Our analytic results are universally applicable for any lattice geometry and spin-length S . We provide precomputed and easy-to-use building blocks for Ising, Heisenberg and transverse field Ising models in the symmetry-unbroken regime. We showcase the quality and simplicity of the method by computing magnetic phase boundaries and excitations gaps. We also treat the Dicke-Ising model of ground-state superradiance where we show that corrections to the MF phase boundary vanish.

DOI: [10.1103/PhysRevA.110.063301](https://doi.org/10.1103/PhysRevA.110.063301)

I. INTRODUCTION

The past decade has witnessed tremendous progress at the intersection points of cold atomic physics, quantum optics and many-body physics. Atoms and ions can be confined in spatially structured arrangements [1–4] and brought into interaction using tailored potentials or cavity-mediated forces [5–7]. This has opened a new window for the exploration of equilibrium and nonequilibrium phenomena, including phase transitions in arrays of trapped Rydberg atoms [8] and Wigner crystals of trapped ions [9,10], super- and subradiance in dense atomic gases [11,12], or exotic time-crystal phases in atom-cavity systems [13,14].

One commonality of these quantum optical platforms is that their essential physics is often captured by many-body models whose microscopic degrees of freedom are quantum spins. However, the structure of the underlying spin-spin couplings is strikingly different to the short-range interactions encountered in solid-state-based quantum magnetism [15]. This is due to the spatially extended nature of the mode functions of photons (phonons) that mediate the interactions between atoms (ions) and thereby give rise to tunable long-range and even all-to-all spin-spin couplings [16–20], see Fig. 1.

In this theoretical work we are concerned with the treatment of such highly connected spin Hamiltonians, motivated but not limited to the above-discussed quantum optical many-body models. Concretely, we will consider general lattice

spin- S Hamiltonians with bilinear couplings, that is,

$$H = -h \sum_i S_i^z + \sum_{i < i'} \sum_{\gamma, \gamma' \in \{+, -, z\}} J_{ii'}^{\gamma\gamma'} S_i^\gamma S_{i'}^{\gamma'}, \quad (1)$$

where S_i^γ represents, for the i th spin, its component along the z direction and the spin ladder operators for $\gamma = z$ and $\gamma = +, -$, respectively. Moreover, $J_{ii'}^{\gamma\gamma'}$ are the coupling constants between spins at lattice sites i and i' , which may be anisotropic in the spin components and which, in cold atomic experiments, can be controlled by geometry and choice of electronic states. Finally, the homogeneous field h may be generated and controlled, for example, by laser-induced level shifts.

Our goal is to investigate the properties of the equilibrium state of these models. We assume this state to be thermal and characterized by a finite temperature $T \geq 0$, see, e.g., Ref. [21] for the demonstration of such a thermometry approach to recent experimental correlation data from a Rydberg-array experiment [22]. This is certainly an approximation for quantum optical spin systems, which are well isolated from the environment (in the sense that they are not embedded in a solid-state matrix). Nevertheless, when preparing ground states and also excited states there is a residual entropy, manifesting in fluctuations, albeit not necessarily thermal.

One recurrent quest in this field is to obtain phase diagrams, which can be probed in experiment, e.g., in Rydberg

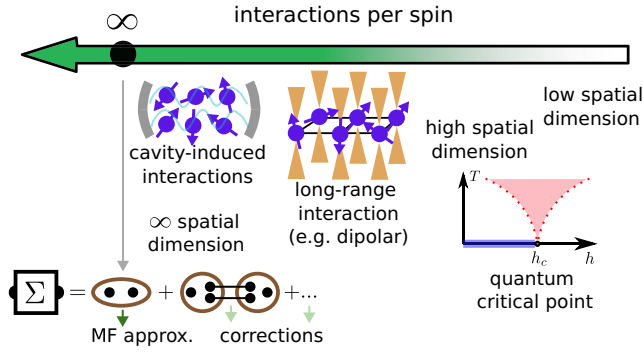


FIG. 1. The validity of the MF approximation in spin systems depends on the number of interactions per spin (green arrow) and is only exact in the limit of infinite connectivity. Corrections to MF can be moderate in systems if the connectivity of spins is large, a common situation in many-body quantum optics, but also in high spatial dimensions or at quantum critical points. In this regime the diagrammatic method proposed in this work provides accurate results at negligible computational cost.

tweezer arrays [22]. More recently, also dynamic quantities such as excitation spectra have come into reach [23]. Theoretically, these and other observables can be obtained from two-point spin correlators, see Eq. (7) below. For example, (second-order) phase transitions are signaled by a divergence of the static correlator [24].

On the computational side, however, a large number of interaction partners per spin often causes considerable difficulties: The plain high-temperature expansion of static correlators [25] becomes ineffective (see, however, Ref. [26]), and approaches relying on finite simulation volumes, e.g., density matrix renormalization group (DMRG) and quantum Monte Carlo (QMC), often suffer from finite-size effects. Furthermore, these methods may be negatively affected by high dimensionality ($d > 1$) or the sign problem [24].

As a complementary and simple method, mean-field (MF) theory is routinely applied. It amounts to approximating the full Hamiltonian (1) by a noninteracting trial Hamiltonian with variational parameters chosen to optimize the free energy [27] (see also Ref. [28] for an insightful discussion). This procedure is often cut short by applying the mnemonically intuitive replacement

$$S_i^\gamma S_{i'}^{\gamma'} \rightarrow S_i^\gamma \langle S_{i'}^{\gamma'} \rangle + \langle S_i^\gamma \rangle S_{i'}^{\gamma'} - \langle S_i^\gamma \rangle \langle S_{i'}^{\gamma'} \rangle \quad (2)$$

to the interaction term in Hamiltonian (1), followed by a self-consistent determination of $\langle S_i^\gamma \rangle$.

In the limit of infinite connectivity, the MF approximation is quantitatively exact [29–31]. Examples are all-to-all interactions (e.g., cavity mediated in the limit of an infinite number of spins [32,33]) or the limit of infinite dimension. However, more realistic Hamiltonians feature a large but finite connectivity, so that the MF approximation is expected to be qualitatively correct [34]. This regime, which, as argued above, is naturally realized in many quantum optical spin systems is the main focus of this work. We show that the spin-spin correlator and the derived observables such as phase boundaries or excitation gaps, can be well approximated by a simple and computationally inexpensive spin-diagrammatic

approach. This rests on an expansion in powers of a suitably defined small parameter, which varies from one problem to another. Importantly, we show that our approach also works at $T = 0$ where at quantum critical points the (effective) dimensionality is increased [35].

We build on foundations of the diagrammatic technique for general quantum spin- S systems, which were laid starting from the late 1960s [36–41]. In Sec. II, we review the basic idea of the method and introduce an efficient way to evaluate the diagrams to unprecedented order. For concreteness and simplicity, we specialize to specific types of spin-spin interactions in Eq. (1). In Sec. III we provide explicit expressions for the two-point functions of $h = 0$ Heisenberg models and the Ising and transverse-field Ising model (TFIM), the latter at $T = 0$. Throughout we stay in the symmetry unbroken regime for simplicity. In Sec. IV we benchmark our method on the hypercubic lattice with nearest-neighbor interactions. Finally, in Sec. V, we apply our method to two particular quantum optical many-body systems with $S = 1/2$, both on the square lattice: A power-law interacting ferromagnetic (FM) Heisenberg model at $T > 0$ [42] and the Dicke-Ising model at $T = 0$ [43,44]. We conclude in Sec. VI.

II. DIAGRAMMATIC TECHNIQUE FOR QUANTUM SPINS VIA KERNEL FUNCTIONS

A. Models and perturbative expansion

We consider $SU(2)$ quantum spin- S operators $\mathbf{S}_j = (S_j^x, S_j^y, S_j^z)^T$ on a lattice with N sites labeled by index j . The operators obey the spin algebra

$$[S_{j_1}^{\alpha_1}, S_{j_2}^{\alpha_2}] = i\delta_{j_1 j_2} \epsilon^{\alpha_1 \alpha_2 \alpha_3} S_{j_1}^{\alpha_3} \quad (3)$$

with $\alpha_{1,2,3} \in \{x, y, z\}$ and the spin-length operator constraint $\mathbf{S}_j \cdot \mathbf{S}_j = S(S+1)$. The general bilinear spin Hamiltonian with homogeneous magnetic field h in z direction is given in Eq. (1) where $S^\pm = (S^x \pm iS^y)/\sqrt{2}$ are the spin ladder operators. In the following, it is understood that $\alpha \in \{x, y, z\}$ while $\gamma \in \{+, -, z\}$.

In the following, we specialize Eq. (1) to three important model classes defined by particular combinations of h and the 3×3 matrix $J_{ii'}^{\gamma\gamma'}$ in flavor space. This specialization is not required by methodological restrictions but was chosen to keep the notation and diagrammatic complexity at a level suitable for presentation. Finally, in Sec. VB we consider a model with a more complicated structure.

The three simple choices correspond to the following standard spin models: (i) The Ising model (which is classical and treated mainly for reference)

$$H = \sum_{i < i'} J_{ii'} S_i^z S_{i'}^z \quad (4)$$

is obtained from Eq. (1) by setting $h = 0$ and $J_{ii'}^{\gamma\gamma'} = \delta_{\gamma,z} \delta_{\gamma',z} J_{ii'}$. (ii) The transverse field Ising model (TFIM)

$$H = \sum_{i < i'} J_{ii'} S_i^x S_{i'}^x - h \sum_i S_i^z \quad (5)$$

corresponds to $J_{ii'}^{\gamma\gamma'} = \frac{1}{2}(1 - \delta_{\gamma,z})(1 - \delta_{\gamma',z})J_{ii'}$. Note that Ising models are usually defined only for $S = 1/2$. (iii) The

Heisenberg model

$$H = \sum_{i<i'} J_{ii'} \mathbf{S}_i \cdot \mathbf{S}_{i'} \quad (6)$$

results from $h = 0$ and $J_{ii'}^{\gamma\gamma'} = \delta_{\bar{\gamma},\gamma'} J_{ii'}$ where we define $\bar{\gamma}$ by $\bar{+} = -$, $\bar{-} = +$, and $\bar{z} = z$. We keep S general and assume vanishing on-site coupling $J_{ii} = 0$ for simplicity.

In the remainder of this work, our computational focus will be on the Matsubara spin-spin correlation function,

$$G_{jj'}^{\alpha\alpha}(iv_m) = T \int_0^\beta d\tau d\tau' e^{iv_m(\tau-\tau')} G_{jj'}^{\alpha\alpha}(\tau, \tau'), \quad (7)$$

where τ is (imaginary) time, $\beta = 1/T$ is the inverse temperature, $v_m = 2\pi Tm$ with $m \in \mathbb{Z}$ a (bosonic) Matsubara frequency, and

$$G_{jj'}^{\alpha\alpha}(\tau, \tau') = \langle \mathcal{T} S_j^\alpha(\tau) S_{j'}^\alpha(\tau') \rangle = G_{jj'}^{\alpha\alpha}(\tau - \tau') \quad (8)$$

the time-ordered (\mathcal{T}) thermal correlation function [41], which only depends on the time difference. Time ordering for spin operators is defined via

$$\mathcal{T} S_j^\alpha(\tau) S_{j'}^{\alpha'}(\tau') = \begin{cases} S_j^\alpha(\tau) S_{j'}^{\alpha'}(\tau') & : \tau > \tau', \\ S_{j'}^{\alpha'}(\tau') S_j^\alpha(\tau) & : \tau' > \tau, \end{cases} \quad (9)$$

and operators in imaginary-time Heisenberg picture are written as $S_j^\alpha(\tau) = e^{H\tau} S_j^\alpha e^{-H\tau}$. Thermal averages are defined as $\langle \dots \rangle = \mathcal{Z}^{-1} \text{Tr}[e^{-\beta H} \dots]$ where $\mathcal{Z} = \text{Tr}e^{-\beta H}$ is the partition function.

While dynamic observables are encoded in the analytically continued version of Eq. (7), $G_{jj'}^{\alpha\alpha}(iv_m \rightarrow v \pm i\eta)$, we will be mainly concerned with the detection of magnetic phase transitions of second-order (continuous) nature. Such a transition towards an ordered phase (with $\langle S_i^\alpha \rangle \neq 0$, say) can be conveniently detected coming from the paramagnetic side without spontaneous symmetry breaking, see the black arrow in Fig. 2(a). According to isothermal linear response theory, it is signaled by a divergent spatial Fourier transform (at ordering wave vector \mathbf{Q}) of the static Matsubara spin-spin correlator [Eq. (7) with $v_m = 0$] also known as spin susceptibility [24]. Note that around first-order (discontinuous) transitions, where the order parameter jumps, the susceptibility is not defined. The analysis or detection of first-order transitions is beyond the scope of this work.

Given these considerations, in the following we will focus on this symmetry-unbroken phase and consider the Matsubara correlator (7) for α for which $\langle S_i^\alpha \rangle = 0$. Among other simplifications on the diagrammatic side to be discussed below, this choice ensures the equality of connected and disconnected two-point correlators.

Next, we review the diagrammatic series expansion of $G_{jj'}^{\alpha\alpha}(iv_m)$ in exchange interaction J , originally developed for the case of quantum spins in Refs. [36–40] and summarized in Ref. [41]. Earlier work on the (classical) Ising model can be found in Refs. [29,45,46]. As usual in perturbation theory [27], we start by splitting the Hamiltonian in interacting and noninteracting parts. For the general spin Hamiltonian (1), we thus set $H = H_{0,h} - V$ where

$$H_{0,h} = -h \sum_i S_i^z, \quad V = - \sum_{i<i'} \sum_{\gamma, \gamma' \in \{+, -, z\}} J_{ii'}^{\gamma\gamma'} S_i^\gamma S_{i'}^{\gamma'}. \quad (10)$$

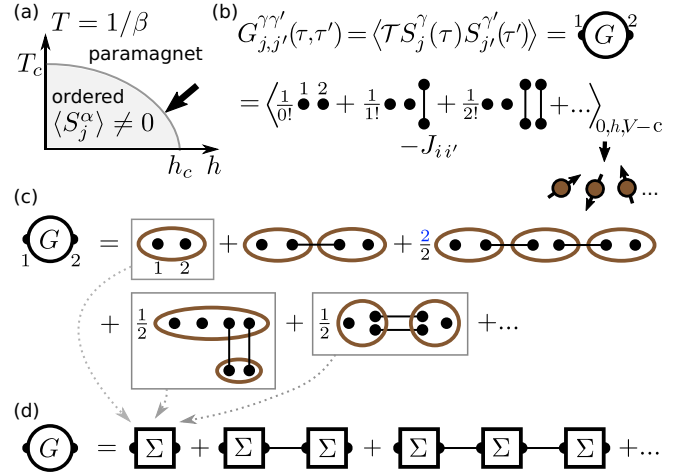


FIG. 2. (a) Schematic of a typical phase diagram for Hamiltonian (1). In this work we approach the magnetic ordering transition from the paramagnetic phase. (b) Diagrammatic representation of the expansion for the spin-spin correlator G in the exchange interaction $-J$ (lines), the orders $n = 0, 1, 2$ are shown explicitly. (c) Diagrammatic representation of the V -connected correlators in (b) in terms of ordinary connected free-spin correlators (brown ellipses). The $1-J$ -irreducible diagrams of order J^0 and J^2 are marked with boxes, the infinite sum of all these diagrams constitutes Σ , the $1-J$ -irreducible part of G . (d) The Larkin equation re-combines Σ and J to form G .

The formal series expansion in $V \sim J$ reads [27]

$$G_{jj'}^{\gamma\gamma'}(\tau, \tau') = \sum_{n=0}^{\infty} \frac{1}{n!} \int_0^\beta d\tau_1 \dots d\tau_n \times \langle \mathcal{T} V(\tau_1) \dots V(\tau_n) S_j^\gamma(\tau) S_{j'}^{\gamma'}(\tau') \rangle_{0,h,V-c}. \quad (11)$$

Here, the averages and time evolution of operators are governed only by $H_{0,h}$ (we avoid a new symbol since no confusion is possible from here on). For the correlator G , we changed to flavor indices $\gamma, \gamma' \in \{+, -, z\}$ adapted to the $U(1)$ symmetry of $H_{0,h}$. This will prove convenient below. The subscript $V-c$ for the averages on the right-hand side of Eq. (11) excludes vacuum contributions [47] where in a diagrammatic interpretation one or more $V(\tau)$ are not connected to the external indices after performing the average. We refer to Appendix A for a rigorous definition. Note that a formula analogous to Eq. (11) applies for any time-ordered product of Heisenberg-picture operators and in particular also for the local magnetization $\langle \mathcal{T} S_j^\alpha(\tau) \rangle = \langle S_j^\alpha \rangle$. However, as mentioned above, in this work we will focus only on two-point functions.

Finally we perform the τ, τ' integral over Eq. (11) to obtain the Matsubara correlator (7) and also specialize to a fixed expansion order n indicated by a superscript,

$$G_{jj'}^{\gamma\gamma'(n)}(iv_m) = T \frac{1}{n!} \int_0^\beta e^{iv_m(\tau-\tau')} d\tau_1 \dots d\tau_n d\tau d\tau' \times \langle \mathcal{T} V(\tau_1) \dots V(\tau_n) S_j^\gamma(\tau) S_{j'}^{\gamma'}(\tau') \rangle_{0,h,V-c}. \quad (12)$$

B. Diagrams, J reducibility, and MF approximation

We proceed with the evaluation of Eq. (12) by a diagrammatic approach [41]. This is conceptually simple, physically

transparent and allows for various subsequent approximation and resummation schemes, one of which will be essential later. In the following, we review the diagrammatic method, the concept of J reducibility and its relation to the MF approximation (2). In the next section, we will propose an evaluation scheme of the diagrams that provides analytical expressions at high orders J^n .

The diagrammatic formulation starts from the graphical representation of Eq. (11) in Fig. 2(b). The dots represent spin operators and for now we do not perform the Fourier transform to Matsubara frequency. The two external spin operators carry multi-indices $1 = (\gamma, j, \tau)$ and $2 = (\gamma', j', \tau')$. All other (internal) spin operators coming from V appear pairwise connected by interaction lines representing $-J_{ik}i_k$, $k = 1, 2, \dots, n$. Flavors, times, and sites of the internal spin operators are summed (or integrated) over and the leading factor $1/n!$ is written explicitly. Interaction lines connect spin operators at the same time (unless retarded, cf. Sec. VB).

Next, the V -connected free spin average in Eq. (11) is taken by colocalizing the $2 + 2n$ spin operators (dots) in any possible way involving blocks of $m = 2, 3, 4, \dots$ spins shown as brown ellipses, see Fig. 2(c) [41]. These blocks represent connected equal-site time-ordered free spin correlators,

$$\langle \mathcal{T} S_i^{\gamma_1}(\tau_1) \dots S_i^{\gamma_m}(\tau_m) \rangle_{0,c,h} = G_{0,c,h}^{\gamma_1 \dots \gamma_m}(\tau_1, \dots, \tau_m), \quad (13)$$

which, for the particular noninteracting Hamiltonian $H_{0,h}$ that we consider in Eq. (10), do not depend on the site index i . Connected spin correlators (with subscript c) are defined in analogy to their V -connected counterparts, see Appendix A. Due to our choice of $J_{ii} = 0$, interaction lines cannot start and end at the same block. In Fig. 2(c), the absence of blocks of size $m = 1$ representing single-spin averages (magnetization) is due to our current focus on the three models in question and on $G^{\alpha\alpha}$ for which $\langle S_i^\alpha \rangle = 0$ in the symmetry-unbroken regime. The presence of blocks of order $m > 2$ signals the absence of Wick's theorem [27] for spin operators, ultimately rooted in the operator-valued right-hand side of the commutation relation (3), which differs from the canonical case of bosonic creation and annihilation operators.

The connected time-ordered free spin correlators of Eq. (13), which are central diagrammatic building blocks will be discussed below in generality. For now, we mention the important special case that arises if all m flavor indices are chosen as z such that all involved operators $S_i^z(\tau_n) = S_i^z$ commute. These connected z -spin correlators are then time independent and given via the order- $(m-1)$ derivative of the Brillouin function $b_c(y)$, which describes the magnetization of a free spin $\langle S^z \rangle$ dependent on $y = \beta h$ [41],

$$G_{0,c,h}^{z \dots z}(\tau_1, \dots, \tau_m) = b_c^{(m-1)}(\beta h), \quad (14)$$

$$b_c(y) = \left(S + \frac{1}{2} \right) \coth \left[\left(S + \frac{1}{2} \right) y \right] - \frac{1}{2} \coth \frac{y}{2}. \quad (15)$$

For $h \rightarrow 0$ we abbreviate $b_c^{(m-1)}(0) \equiv b_{c,m-1}$, e.g., $b_{c,1} = S(S+1)/3$ is the free spin (static) Curie susceptibility that will become important in the following discussion.

Having explained the building blocks of the diagrams in Fig. 2(c), we now turn their topology, i.e., the particular choice of blocks and their connection. Topological multiplicity factors Λ (denoted in blue) appear if the same diagram topology

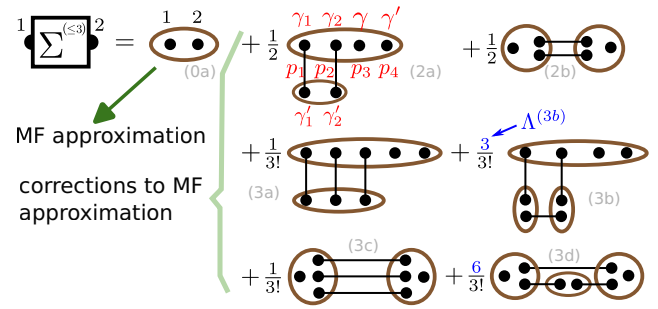


FIG. 3. Diagrams for Σ up to order J^3 for the situation described in the text where magnetization is not relevant. The blue multiplicity factors $\Lambda^{(nx)}$ denote the number of ways to arrive at a given diagram starting from the expansion in Fig. 2(b), e.g., in diagram (3b) there are three choices to pick the bottom line from the three lines available at third-order perturbation theory. The two vertical lines are equivalent and do not enhance the multiplicity as an exchange can be compensated by a permutation of sites within the top ellipse.

can be arrived at by distributing the dots in Fig. 2(b) to the given set of blocks in multiple ways, see, e.g., the last diagram in the first line of Fig. 2(c). Diagrams that only differ by a rearrangement of dots within blocks are not topologically different. Formally, the multiplicity factor can be computed via the number of elements in the automorphism group \mathcal{A}_x of a diagram x of order J^n : $\Lambda = n!/\text{ord}(\mathcal{A}_x)$.

The diagrams in Fig. 2(c) can be classified as either 1- J reducible or 1- J irreducible (1JI). In 1- J reducible diagrams it is possible to separate the external spin operators (single dots) by cutting a single interaction line. If this is not possible, the diagram is 1JI. The infinite sum of all 1JI diagrams is denoted by Σ . For examples, the contributions to Σ of order J^0 and J^2 are indicated with boxes in Fig. 2(c).

All diagrammatic contributions to the spin correlator G that are 1- J reducible can be represented by 1JI diagrams connected by one or more interaction lines, see Fig. 2(d). This diagrammatic expression can be summed exactly and yields the Larkin equation [36,41]. In frequency space, it reads

$$G(iv_m) = [1 + \Sigma(iv_m) \cdot J]^{-1} \cdot \Sigma(iv_m). \quad (16)$$

Here all objects are considered $N \times N$ matrices with two site indices, cf. Eq. (7) and for our purposes the flavors will all be set to a fixed α with $\alpha \in \{x, y, z\}$ for simplicity. Note the similarity of Eq. (16) to Dyson's equation for canonical bosonic or fermionic systems [27], which, however, rests on the concept of cutting free propagator lines (and not interaction lines).

Given the above diagrammatic rules, it is straightforward to write down the 1JI diagrams for Σ at order n indicated by $\Sigma^{(n)}$. The diagrams for $n \leq 3$, which include the boxed diagrams of Fig. 2(b) are shown in Fig. 3. We label the different diagram topologies at order n with an additional index $x = a, b, c, \dots$. Each diagram topology is uniquely identified by (nx) . The diagrams for $\Sigma^{(4)}$ have not been systematically collected so far in literature and are given in Fig. 7 of Appendix D. Note that diagrams that combine the two external operators together with one internal operator in a $m = 3$ block are 1JI by our definition. However, for the particular setup and observables that we focus on in this work (see above), these diagrams vanish.

We conclude this section by linking the diagrammatic expansion to the MF approximation for $G^{\alpha\alpha}$. Quite simply, the latter is obtained by using only the lowest-order approximation for Σ (green arrow in Fig. 3)

$$\Sigma^{\alpha\alpha} \rightarrow \Sigma^{\alpha\alpha(0)} = G_{0,c,h}^{\alpha\alpha}. \quad (17)$$

For $\alpha = z$, this evaluates to $b_c^{(1)}(\beta h)$, see Eq. (14). We also assumed $\langle S_i^\alpha \rangle = 0$, otherwise h in Eq. (17) would need to be replaced by the Weiss field, see Ref. [41] and Sec. VB. The easiest way to see the correspondence between Eq. (17) and the MF approximation is to recall that the latter is exact for $N \rightarrow \infty$ if each spin interacts with all other spins in the system, which requires us to redefine $J \rightarrow J/N$. For G and in the limit $N \rightarrow \infty$, this means that stringlike diagrams as in the first line of Fig. 2(c) are the only finite contribution. This follows since the site indices of the internal ($m = 2$) blocks can be summed freely over all available sites only in stringlike diagrams while being more restricted in diagrams that contain loops. Finally, the stringlike diagrams are exactly the diagrams that are produced by the replacement $\Sigma \rightarrow \Sigma^{(0)}$ in the Larkin equation of Fig. 2(d). It follows that contributions $\Sigma^{(n)}$ with $n > 0$ represent corrections to the MF results, see Figs. 1 and 3.

C. Diagram evaluation via kernel functions

The remaining task is to calculate the analytical expressions encoded in the particular diagrams $\Sigma_{jj'}^{\gamma\gamma'(nx)}(iv_m)$, which represent the different contributions of the right-hand side of Eq. (12). Two observations on the simple nature of the chosen models (Ising, TFIM and Heisenberg, cf. Sec. II A) are helpful but by no means crucial for progress: (i) The values for the blocks [brown ellipses, see Eq. (13)] are site independent and (ii) the coupling between any two blocks is characterized by a single number $J_{ii'}$ (unlike for, say, XXZ interactions). Hence we can combine all $J_{ii'}$ [stemming from the insertions of V , cf. Eq. (10)] along with the site sums in a geometry factor $t_{jj'}^{(nx)}[J] \sim J^n$,

$$\Sigma_{jj'}^{\gamma\gamma'(nx)}(iv_m) \equiv t_{jj'}^{(nx)}[J] \cdot \sigma^{\gamma\gamma'(nx)}(iv_m). \quad (18)$$

This geometry factor captures the dependence of the particular diagram (nx) on j, j' and the underlying $N \times N$ coupling matrix $J_{ii'}$. For example, with regard to Fig. 3, the geometry factor for diagram (0a) is simply $\delta_{jj'}$ whereas for (2a) and (2b) we read off

$$t_{jj'}^{(2a)} = \delta_{jj'} \sum_i J_{ji} J_{ij}, \quad t_{jj'}^{(2b)} = (J_{jj'})^2. \quad (19)$$

The geometry factors for all diagrams of order $n = 0, 2, 3$ are shown in the second column in Table I. In the third column, we provide the momentum space representation for translation invariant lattices with spatial Fourier transform defined by

$$J_{\mathbf{k}} = \sum_{\mathbf{r}_j} e^{-i\mathbf{k}\cdot\mathbf{r}_j} J_{0,\mathbf{r}_j}, \quad (20)$$

and analogous for $G_{\mathbf{k}}$ and $\Sigma_{\mathbf{k}}$. In the fourth column we specialize to the infinite ($N \rightarrow \infty$) nearest-neighbor hypercubic lattice model in d spatial dimensions, see the caption of

TABLE I. Geometry factors $t^{(nx)}[J]$ for Σ diagrams of order $n = 0, 2, 3$ and all topologies (for the case $n = 4$ see Table VI). Results in the second column are given in real space [where $J_{jj'}^2$ is understood as $(J_{jj'})^2$ etc.]. The third column shows the same results in momentum space (where we abbreviate $\int_{\mathbf{q}} = 1/N \sum_{\mathbf{q}}$). In the fourth column, momentum space results are specialized for an infinite d -dimensional hypercubic lattice with a lattice constant of unity and nearest-neighbor coupling J_1 where $\tilde{J}_{\mathbf{k}} \equiv 2J_1 \sum_{\mu=1}^d \cos k_{\mu}$ and accordingly $\tilde{J}_0 = 2dJ_1$.

| top. | r space $t_{jj'}^{(nx)}$ | k space $t_{\mathbf{k}}^{(nx)}$ | nn-hyp. $\tilde{t}_{\mathbf{k}}^{(nx)}$ |
|------|---|---|---|
| (0a) | $\delta_{jj'}$ | 1 | 1 |
| (2a) | $\delta_{jj'} [J \cdot J]_{jj'}$ | $\int_{\mathbf{q}} J_{\mathbf{q}}^2$ | $J_1 \tilde{J}_0$ |
| (2b) | $J_{jj'}^2$ | $\int_{\mathbf{q}} J_{\mathbf{q}-\mathbf{k}} J_{\mathbf{q}}$ | $J_1 \tilde{J}_{\mathbf{k}}$ |
| (3a) | $\delta_{jj'} \sum_i J_{ji}^3$ | $\int_{\mathbf{p},\mathbf{q}} J_{\mathbf{p}} J_{\mathbf{q}} J_{\mathbf{p}+\mathbf{q}}$ | $J_1^2 \tilde{J}_0$ |
| (3b) | $\delta_{jj'} [J \cdot J \cdot J]_{jj}$ | $\int_{\mathbf{q}} J_{\mathbf{q}}^3$ | 0 |
| (3c) | $J_{jj'}^3$ | $\int_{\mathbf{p},\mathbf{q}} J_{\mathbf{p}-\mathbf{k}} J_{\mathbf{q}} J_{\mathbf{p}+\mathbf{q}}$ | $J_1^2 \tilde{J}_{\mathbf{k}}$ |
| (3d) | $J_{jj'} [J \cdot J]_{jj'}$ | $\int_{\mathbf{q}} J_{\mathbf{k}-\mathbf{q}} J_{\mathbf{q}}^2$ | 0 |

Table I for more details. Geometry factors for the fourth-order diagrams $\Sigma^{(4)}$ are summarized in Table VI of Appendix D.

Beyond the frequency independent geometry factor, the remaining contribution in Eq. (18) denoted as $\sigma^{(nx)}(iv_m)$ only depends on the type of spin model (here: Ising, TFIM, Heisenberg). We define it to include the topological multiplicity factor $\Lambda^{(nx)}$ of the diagram (nx). In principle, obtaining $\sigma^{(nx)}$ is straightforward in frequency space [41] where interaction lines proportional to $\delta_{v_i+v_{i'}}$ connect the blocks, which are temporal Fourier transforms of Eq. (13), $G_{0,c,h}^{\gamma_1 \dots \gamma_m}(\omega_1, \dots, \omega_{m-1})$. The latter, however, are difficult to calculate in general beyond the case $\gamma_1 = \dots = \gamma_m = z$ [see Eq. (14)], especially for $h = 0$ where a distinction of cases regarding various frequency combinations is required. Despite recent algorithmic advances [48,49] the general $G_{0,c,h}^{\gamma_1 \dots \gamma_m}(\omega_1, \dots, \omega_{m-1})$ (which beyond their appearance in perturbation theory lack physical significance for large m) are currently known analytically up to order $m = 4$ [41]. This would only suffice to compute Σ to order J^2 . On the other hand, without the temporal Fourier transform and for a fixed order of times, the blocks representing $\langle \mathcal{T} S^{\gamma_1}(\tau_1) \dots S^{\gamma_m}(\tau_m) \rangle_{0,c,h}$ [cf. Eq. (13)] simplify to standard connected free-spin equal-time averages $\langle S^{\gamma_1} \dots S^{\gamma_m} \rangle_{0,c,h}$, which can be efficiently computed for general S , see Sec. 6.2 in Ref. [49].

To make progress, the crucial reformulation detailed in Appendix B expresses $\sigma^{(nx)}$ such that only the simple $\langle S^{\gamma_1} \dots S^{\gamma_m} \rangle_{0,c,h}$ are required. All the remaining complexity is encapsulated in the universal (model-independent) kernel functions $K_{n+2}(\Omega_1, \dots, \Omega_{n+2})$ of Ref. [49]. The latter originally appeared in the context of Fourier transforms of time-ordered correlation functions. The key point is that an n th-order perturbative expression as in Eq. (12) can be understood as a Fourier transform of a time-ordered correlation function of order $n + 2$ with n frequencies set to zero.

The translation of diagram (nx) to an expression $\sigma^{(nx)}$ is straightforward. To avoid unnecessary complicated notation,

we just give two examples: For diagram (2a), with the labeling of internal times and flavors in Fig. 3 (red), one obtains

$$\begin{aligned} \sigma^{\gamma\gamma'(2a)}(iv_m) &= \Lambda^{(2a)} \frac{(-1)^n}{n!} \sum_{\gamma_{1,\dots,n}^{(i)}} \sum_{p \in S_{n+2}} K_{n+2}(\mathcal{P}\{\Omega_1(p_1), \dots, \Omega_{n+2}(p_{n+2})\}) \\ &\quad \times \langle \mathcal{P}S^{\gamma_1}(p_1)S^{\gamma_2}(p_2)S^{\gamma}(p_3)S^{\gamma'}(p_4) \rangle_{0,c,h} \langle \mathcal{P}S^{\gamma'_1}(p_1)S^{\gamma'_2}(p_2) \rangle_{0,c,h}, \end{aligned} \quad (21)$$

where $\Lambda^{(2a)} = 1$ and $n = 2$. As another example, diagram (3b) with $\Lambda^{(3b)} = 3$ and $n = 3$ is

$$\begin{aligned} \sigma^{\gamma\gamma'(3b)}(iv_m) &= \Lambda^{(3b)} \frac{(-1)^n}{n!} \sum_{\gamma_{1,\dots,n}^{(i)}} \sum_{p \in S_{n+2}} K_{n+2}(\mathcal{P}\{\Omega_1(p_1), \dots, \Omega_{n+2}(p_{n+2})\}) \\ &\quad \times \langle \mathcal{P}S^{\gamma_1}(p_1)S^{\gamma_2}(p_2)S^{\gamma}(p_4)S^{\gamma'}(p_5) \rangle_{0,c,h} \langle \mathcal{P}S^{\gamma'_1}(p_1)S^{\gamma'_3}(p_3) \rangle_{0,c,h} \langle \mathcal{P}S^{\gamma'_2}(p_2)S^{\gamma'_5}(p_5) \rangle_{0,c,h}. \end{aligned} \quad (22)$$

The internal flavor sums over $\gamma_{1,\dots,n}^{(i)}$ depend on the model, e.g., for the Heisenberg case these sums are over $\{+, -, z\}$ while restricted to $\{z\}$ in the Ising case. The second sum is over the $(n+2)!$ permutations S_{n+2} that determine the ordering of both the argument list of K_{n+2} and the spin operators in the equal-time averages. This is accomplished by the index ordering operator \mathcal{P} . This operator applies to operator strings and argument lists alike. It acts like time-ordering, but for discrete indices $(1), (2), \dots, (n+2)$ that, unlike imaginary time arguments, do not affect the operator, for example $\mathcal{P}S^+(1)S^-(3)S^z(2) = S^-S^zS^+$. Finally, the Ω list is given by

$$\{\Omega_1, \dots, \Omega_n, \Omega_{n+1}, \Omega_{n+2}\} = \{-(\gamma_1 + \gamma'_1)h, \dots, -(\gamma_n + \gamma'_n)h, iv_m - \gamma h, -iv_m - \gamma' h\}, \quad (23)$$

where the following replacement rule for flavor labels is understood: $\{z, +, -\} \rightarrow \{0, +1, -1\}$.

Closed-form expressions for general kernel functions $K_k(\Omega_1, \dots, \Omega_k)$ can be found in Ref. [49]. The expressions grow in complexity with k , however, for the current application with the specific form of the Ω list in Eq. (23) and our focus on either $h = 0$ (Ising and Heisenberg models) or $T \rightarrow 0$ (for the TFIM), the kernel functions simplify considerably. The resulting expressions are given in Appendix C.

Expressions analogous to Eqs. (21) and (22) can be straightforwardly written for all diagram topologies and should be evaluated via computer algebra for efficiency. In the next section, we provide the expressions for $\sigma^{\gamma\gamma'(nx)}(iv_m)$ obtained in this way. Finally, the sum over all topologies yields $\Sigma^{(n)}$ at order J^n ,

$$\Sigma_{jj'}^{\gamma\gamma'(n)}(iv_m) = \sum_{x=a,b,c,\dots} t_{jj'}^{(nx)}[J] \sigma^{\gamma\gamma'(nx)}(iv_m). \quad (24)$$

III. ANALYTIC RESULTS FOR 1-J IRREDUCIBLE DIAGRAMS

In this section we report the analytic results of the diagram evaluation up to third order in J for the Ising model, TFIM at $T = 0$ and the Heisenberg model as defined in Eqs. (4), (5) and (6). Diagrams in fourth order and their analytic results are relegated to Appendix D.

We provide results for the second contribution to Eq. (18), the geometry independent $\sigma^{\gamma\gamma'(nx)}(iv_m)$. For the Ising model and TFIM case we consider σ^{zz} and σ^{xx} , respectively, see Table II. In both cases diagrams, which involve blocks of any odd order vanish and are not listed. For the Ising model this is due to spin flip symmetry $S_i^z \rightarrow -S_i^z \forall i$ in the paramagnetic phase, for the σ^{xx} in the TFIM this follows from the fact that the blocks solely involve S^+ and S^- , which need to appear in equal numbers for any finite contribution in light of $U(1)$

spin rotation symmetry of $H_{0,h}$. For the Ising model only static contributions are finite due to its classical nature.

The results for $\Sigma_{jj'}^{\gamma\gamma'(n)}(iv_m)$ computed by summing over topologies [Eq. (24)] have been tested for small clusters of spins, e.g., for the dimer with $N = 2$ and $J_{12} = J_{21} = J_1$ and $J_{11} = J_{22} = 0$. In this case, for moderately large S , the Hilbert space is small and the exact two-point function G can be found using the spectral representation [27]. Hence the exact Σ is obtained via Eq. (16). This exact result is then expanded in J_1 and checked against $\Sigma_{jj'}^{\gamma\gamma'(n)}(iv_m)$ computed diagrammatically. As an example, for the TFIM dimer with $J_1 > 0$, $T = 0$ and $S = 1/2$, one confirms

$$\begin{aligned} \Sigma_{11}^{xx}(iv) &= \frac{h}{2(h^2 + v^2)} - J_1^2 \frac{5h^2 + v^2}{64h(h^2 + v^2)^2} \\ &\quad + J_1^4 \frac{(43h^4 + 14h^2v^2 + 3v^4)}{4096h^3(h^2 + v^2)^3} + O(J_1^6), \end{aligned} \quad (25)$$

$$\Sigma_{12}^{xx}(iv) = J_1^3 \frac{-1}{64h(h^2 + v^2)^2} + O(J_1^5). \quad (26)$$

TABLE II. Ising model and TFIM at $T = 0$, both in the symmetric phase: Expansion of the lattice independent parts $\sigma^{(nx)}$ of the diagrams $\Sigma^{(nx)}$ for $n = 0, 2, 3$ [cf. Eq. (18)]. Only topologies with finite $\sigma^{(nx)}$ are shown. The derivatives of the Brillouin function (15) at zero field are denoted by $b_c^{(m)}(0) \equiv b_{c,m}$. Fourth-order results are given in Table VII.

| | Ising $T^{1+n} \sigma^{zz(nx)}(iv_m = 0)$ | TFIM $\sigma^{xx(nx)}(iv) _{T=0}$ |
|------|---|--|
| (0a) | $b_{c,1}$ | $\frac{hS}{h^2+v^2}$ |
| (2a) | $\frac{1}{2} b_{c,1} b_{c,3}$ | $\frac{-S^2(5h^2+v^2)}{16h(h^2+v^2)^2}$ |
| (3b) | $-\frac{1}{2} b_{c,1}^2 b_{c,3}$ | $\frac{S^3(4h^2+v^2)}{16h^2(h^2+v^2)^2}$ |
| (3c) | $-\frac{1}{6} b_{c,3}^2$ | $\frac{-S^2}{16(h^2+v^2)^2}$ |

TABLE III. Heisenberg model at $T > 0$ in the paramagnetic phase: Expansion of the lattice independent parts $\sigma^{(nx)}$ of the diagrams $\Sigma^{(nx)}$ for $n = 0, 2, 3$, cf. Eq. (18). Fourth-order results are given in Table VII. The Δ in the dynamic case stands for $1/(2\pi m)$.

| $T^{1+n} \sigma^{zz(nx)}$ | static ($v_m = 0$) | dyn. ($v_m \neq 0$) |
|---------------------------|---|----------------------------------|
| (0a) | $b_{c,1}$ | 0 |
| (2a) | $\frac{b_{c,1}^2}{-6}(1 + 6b_{c,1})$ | $+2\Delta^2 b_{c,1}^2$ |
| (2b) | $\frac{b_{c,1}^2}{-12}$ | $-2\Delta^2 b_{c,1}^2$ |
| (3a) | $\frac{b_{c,1}^2}{-24}(1 + 4b_{c,1})$ | $+\frac{1}{2}\Delta^2 b_{c,1}^2$ |
| (3b) | $\frac{b_{c,1}^3}{6}(1 + 6b_{c,1})$ | $-2\Delta^2 b_{c,1}^3$ |
| (3c) | $\frac{b_{c,1}^2}{-120}(48b_{c,1}^2 + 16b_{c,1} + 3)$ | $-\frac{1}{2}\Delta^2 b_{c,1}^2$ |
| (3d) | 0 | $+2\Delta^2 b_{c,1}^3$ |

As some diagrams like (3b) vanish for the dimer geometry it is important to also check the fully connected trimer with $N = 3$ in an analogous fashion.

Finally, we turn to the Heisenberg case at $T > 0$ where the $\sigma^{z\alpha(nx)} = \sigma^{\alpha\alpha(nx)}$ are reported in Table III. We need to distinguish between the static case $v_m = 0$ and the dynamic case $v_m = 2\pi mT \neq 0$ for which we abbreviate $\Delta = \frac{1}{2\pi m}$. Again, these results have been tested for small spin clusters. Another nontrivial check for the resulting $\Sigma^{(n)}$ is the fulfillment of $\Sigma_{\mathbf{k}=0}^{(n)}(iv_m \neq 0) = 0$ required by the constant-of-motion property of $S_{\mathbf{k}=0}^z$ in a Heisenberg system.

IV. HYPERCUBIC LATTICE BENCHMARKS

We now proceed to test the applicability of the diagrammatic expansion for nearest-neighbor models on the hypercubic lattice in d spatial dimensions with AFM coupling $J_1 > 0$. The geometry factors and further details on the lattice can be found in Table I. For the Ising and Heisenberg case we focus on the magnetic ordering temperature T_c and for the TFIM at $T = 0$ we consider the critical field h_c and the excitation gap $\Delta(h)$. The latter serves as an example for a dynamical quantity, which needs to be evaluated via analytical continuation. We will use the inverse dimension $1/d$ as a small control parameter.

The magnetic phase boundary is signaled by the divergence of the static susceptibility, according to Eq. (16),

$$G_{\mathbf{k}}^{-1}(iv_m = 0) = 1/\Sigma_{\mathbf{k}}(iv_m = 0) + J_{\mathbf{k}} \stackrel{!}{=} 0, \quad (27)$$

TABLE IV. Nonvanishing geometry factors $\beta^n \tilde{t}_{\mathbf{k}=\mathbf{N}}^{(nx)}[J]$ ($n \leq 4$) for the nearest-neighbor d -dimensional hypercubic lattice with coupling J_1 as a function of $X_1 = \beta J_1$. The leading-order scaling in powers of $1/d$ close to the thermal ordering transition is provided next to the diagram label. Geometry factors for $n > 4$ (not shown) are of order d^{-3} or smaller.

| | | | | |
|--------------------|--------------------|--------------------|--------------------|--------------------|
| (0a) $\sim d^0$ | (2a) $\sim d^{-1}$ | (2b) $\sim d^{-1}$ | (3a) $\sim d^{-2}$ | (3c) $\sim d^{-2}$ |
| 1 | $+2dX_1^2$ | $-2dX_1^2$ | $+2dX_1^3$ | $-2dX_1^3$ |
| (4a) $\sim d^{-3}$ | (4b) $\sim d^{-2}$ | (4c) $\sim d^{-3}$ | (4e) $\sim d^{-2}$ | (4f) $\sim d^{-2}$ |
| $+2dX_1^4$ | $+4d^2X_1^4$ | $-2dX_1^4$ | $-8d^2X_1^4$ | $+4d^2X_1^4$ |
| (4h) $\sim d^{-2}$ | (4j) $\sim d^{-2}$ | (4l) $\sim d^{-2}$ | | (4m) $\sim d^{-2}$ |
| $+4d^2X_1^4$ | $6d[2d - 1]X_1^4$ | $6d[2d - 1]X_1^4$ | | $-6d[2d - 1]X_1^4$ |

with \mathbf{k} replaced by the Néel wave vector $\mathbf{N} = (\pi, \pi, \dots, \pi)$. Thus the critical coupling is given by the solution of $0 \stackrel{!}{=} 1/\Sigma_{\mathbf{N}} - 2dJ_1$. We specialize to the thermal transition in the Ising case (with $S = 1/2$) or Heisenberg case. First, as stated before, the MF approximation for T_c is found by replacing $\Sigma_{\mathbf{N}} \rightarrow \Sigma_{\mathbf{N}}^{(0)} = \beta b_{c,1}$ in the above equation, which yields the well-known MF result $T_c^{(0)} = 2d b_{c,1} J_1 \sim d$. We then divide Eq. (27) by T and proceed to obtain corrections to the MF result for T_c . Following pioneering work in Refs. [50,51] we seek a consistent expansion of

$$1/(T\Sigma_{\mathbf{N}}) = 2d\beta J_1 \quad (28)$$

in the parameter $1/d$ assumed to be small. In this case MF is approximately valid so that $X_1 \equiv \beta J_1$ close to criticality is of order $\sim 1/d$. With this in mind we provide the hypercubic geometry factors $\beta^n \tilde{t}_{\mathbf{k}=\mathbf{N}}^{(nx)}$ for all nonvanishing topologies in Table IV. Next to the diagram label we show the leading scaling with $1/d$ of the particular $\beta^n \tilde{t}_{\mathbf{k}=\mathbf{N}}^{(nx)}$ close to the thermal transition, which does depend both on order n and topology x . We can thus expand $1/(T\Sigma_{\mathbf{N}})$ up to order $(1/d)^m$, drop all higher orders and solve numerically for T_c . Since the $\Sigma^{(n)}$ are available up to $n = 4$, we can consider $m = 0, 1, 2$, cf. Table IV. Explicitly, we have

$$\frac{1}{T\Sigma_{\mathbf{N}}} = \frac{1}{T\sigma^{(0)}} - \frac{A_1}{(T\sigma^{(0)})^2} + \frac{A_2}{(T\sigma^{(0)})^3} + O(d^{-3}), \quad (29)$$

$$A_1 = 2dX_1^2 T^3 (\sigma^{(2a)} - \sigma^{(2b)}), \quad (30)$$

$$A_2 = A_1^2 - T^4 \sigma^{(0)} [2dX_1^3 (\sigma^{(3a)} - \sigma^{(3c)}) + 4d^2 X_1^4 T (\sigma^{(4b)} - 2\sigma^{(4e)} + \sigma^{(4f)} + \sigma^{(4h)} + 3\sigma^{(4j)} + 3\sigma^{(4l)} - 3\sigma^{(4m)})], \quad (31)$$

where $A_1 \sim 1/d$ and $A_2 \sim 1/d^2$.

We start with the Ising case, where T_c was already obtained in Ref. [50] up to order $1/d^3$. We report the results for $T_c/T_c^{(0)}$ and $d = 3, \dots, 7$ in Table V. For large d , the quasiexact results from high-order series expansion or Monte Carlo simulations [52–54] are rapidly approached as the order m in $1/d$ is increased. We also compare our results at order $1/d^2$ to other diagrammatic approaches with different resummation strategies: Our results are similar to the spin functional RG approach (spin-fRG) by Krieg and Kopietz [50], only at $d = 3$ the latter has a slight advantage. The dynamical MF theory for spins [55] (spin-DMFT) is not competitive. This is not

TABLE V. Ising model: Critical temperature $T_c/T_c^{(0)}$ for the d -dimensional nearest-neighbor Ising model ($S = 1/2$) on the hypercubic lattice normalized to the MF transition temperature $T_c^{(0)} = dJ_1/2$. The quasiexact benchmark results in the second column [52–54] are compared to the results obtained from Eq. (29) evaluated up to order $1/d$ and $1/d^2$, respectively. For comparison, the last two columns report results from spin-fRG [50] and spin-DMFT [55].

| d | exact | $O(1/d)$ | $O(1/d^2)$ | spin-fRG [50] | spin-DMFT [55] |
|-----|-------|----------|------------|---------------|----------------|
| 3 | 0.752 | 0.789 | 0.740 | 0.744 | 0.659 |
| 4 | 0.835 | 0.854 | 0.839 | 0.839 | 0.807 |
| 5 | 0.878 | 0.887 | 0.880 | 0.880 | 0.865 |
| 6 | 0.903 | 0.908 | 0.904 | 0.904 | |
| 7 | 0.919 | 0.923 | 0.920 | 0.920 | |

surprising given DMFT's local approximation of Σ already fails in order J^3 where the nonlocal diagram (3c) appears.¹

For the Heisenberg model, benchmark checks of T_c suffer from the scarcity of exact results for $d > 3$. The exception is the classical case ($S \rightarrow \infty$) for $d = 4$. Here $T_c/T_c^{(0)}$ improves from 0.8536 in order $1/d$ to 0.8315 in order $1/d^2$ with the exact result at 0.822 [56]. For the case $d = 3$ and $S < \infty$, Eq. (28) often yields nonreal solutions at the limited expansion orders available. An exception is the case $d = 3$, $S = 3/2$ for which $T_c/T_c^{(0)}$ improves from 0.769 in order $1/d$ to 0.657 in order $1/d^2$ somewhat closer to the exact result 0.702 [57].

For the TFIM at $T = 0$, the critical field at the ordering transition is given from Eq. (27) as

$$1/(d\Sigma_{\mathbf{N}}^{xx}) \stackrel{!}{=} 2J_1. \quad (32)$$

The MF approximation with $\Sigma_{\mathbf{N}}^{xx} \rightarrow S/h$ yields $h_c^{(0)} = 2dSJ_1 \sim d$. Using $\sigma^{xx(nx)}(iv=0)|_{T=0} \sim 1/h^{1+n}$ we again ex-

¹Note that the lower-order nonlocal diagram (2b) vanishes for the Ising model.

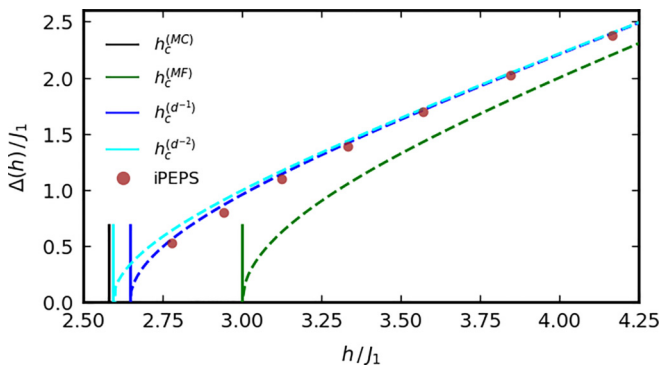


FIG. 4. TFIM on the cubic lattice at $T = 0$ and $S = 1/2$. The vertical lines indicate the critical field h_c in $1/d$ expansion Eq. (32), the quasi-exact result [58] (black) is rapidly approached with increasing expansion order. The same expansion is also used to estimate the spectral gap $\Delta(h)$ shown by dashed lines. The first correction to MF approximation is already in good agreement to the tensor-network (iPEPS) simulation of Ref. [59].

pand the left-hand side for $h \gtrsim h_c$ in orders of $1/d$, which yields expressions similar to Eq. (29). We focus on the case $d = 3$, $S = 1/2$ and report the results for h_c in Fig. 4, see vertical lines. The quasiexact Monte Carlo result $h_c^{(MC)} = 2.57907(3)J_1$ [58] is rapidly approached.

To showcase the advantage of analytical expressions for the Matsubara correlator, we consider the excitation gap $\Delta(h)$ for $h \gtrsim h_c$ which we obtain from the dynamical xx -spin correlator, $G_{\mathbf{k}}^{xx}(iv \neq 0)$. The latter contains the dispersion $\omega_{\mathbf{k}}$ of spin waves transversal to the magnetization in the S^z direction determined from the position of the sharp peak in $\text{Im}G_{\mathbf{k}}^{xx,R}(v)$. The weight of the peak is the one-particle structure factor. For $h \rightarrow h_c$ from above, we expect $\omega_{\mathbf{k}}$ to vanish at $\mathbf{k} = \mathbf{N}$ where the spin wave softens and order sets in. For $h > h_c$, the gap is thus defined as $\Delta(h) = \omega_{\mathbf{N}}$ and we consider

$$G_{\mathbf{N}}^{xx}(iv) = \frac{1/d}{\frac{1}{d\Sigma_{\mathbf{N}}^{xx}(iv)} - 2J_1}. \quad (33)$$

We use an expansion of the denominator similar to above, which we here evaluate to order $1/d$ (and analogously for MF and order $1/d^2$). We find

$$G_{\mathbf{N}}^{xx}(iv) \simeq \frac{hS}{h^2 + \frac{5}{8}dSJ_1^2 - 2dShJ_1 - (iv)^2(1 + \frac{dSJ_1^2}{8h^2})} \quad (34)$$

and after analytic continuation the gap is obtained as

$$\Delta^{(1/d)}(h) = \sqrt{\left(h^2 - 2dShJ_1 + \frac{5}{8}dSJ_1^2\right) / \left(1 + \frac{dSJ_1^2}{8h^2}\right)}. \quad (35)$$

Setting $d = 3$ and $S = 1/2$, this agrees very well with recent iPEPS tensor network simulations in Ref. [59], see Fig. 4 (blue dashed line and dots). For $h \gtrsim h_c$, the iPEPS is actually closer to $\Delta^{(1/d)}(h)$ than to $\Delta^{(1/d^2)}(h)$, we suspect this is an artifact of finite bond dimension of the tensor network.

V. APPLICATION TO MODELS FROM MANY-BODY QUANTUM OPTICS

A. Long-range square lattice Heisenberg model

As a first of two applications inspired from many-body quantum optical systems we consider the $S = 1/2$ Heisenberg square lattice model with long-range FM power-law interactions,

$$J_{i\bar{i}'} = J_1/|\mathbf{r}_i - \mathbf{r}_{i'}|^\alpha, \quad (36)$$

with $J_1 < 0$. This model has been recently studied with QMC simulations [42], which are numerically expensive due to the large system sizes required to approximate the infinite system limit. The lattice constant is set to unity and the interesting regime for the power-law exponent is $\alpha \in (2, 4)$ [31]. In this range α is large enough for a well-defined thermodynamic limit but small enough for a finite FM ordering temperature $T_c > 0$ evading the Mermin-Wagner theorem [60]. We abbreviate $J_{\mathbf{r}_j} = J_1/|\mathbf{r}_j|^\alpha$.

In analogy to Sec. IV, T_c is determined from

$$-\beta J_{\mathbf{k}=\mathbf{0}} \stackrel{!}{=} 1/(T\Sigma_{\mathbf{k}=\mathbf{0}}). \quad (37)$$

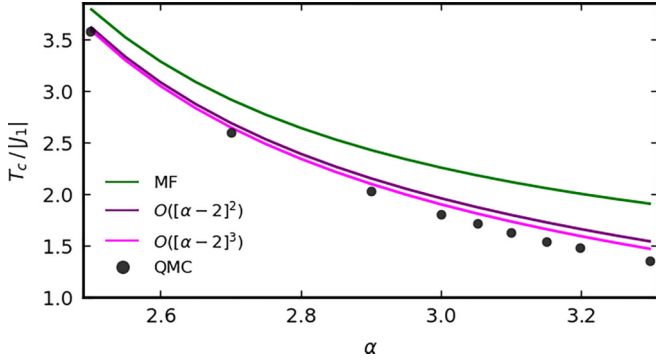


FIG. 5. Ordering temperature for the $S = 1/2$ square lattice Heisenberg FM with couplings decaying as a power law with exponent α , see Eq. (36). Dots denote reference data from QMC taken from Ref. [42]. Colored lines indicate T_c in MF approximation (green), and adding corrections up to order $[\alpha - 2]^2$ (purple) and $[\alpha - 2]^3$ (magenta), respectively.

To compute the spatial Fourier transform $J_{\mathbf{k}=0}$ on the left-hand side and for subsequent expansions on the right-hand side, we obtain numerically the lattice sums $I^{(m)} \equiv \sum_{j \neq 0} r_j^{-\alpha m}$ for $m = 1, 2, 3$ and a sufficiently large cutoff. Then $J_{\mathbf{k}=0} = J_1 I^{(1)}$. To identify a suitable expansion scheme, we consider the integral approximation of $I^{(m)}$ with lower bound $a = O(1)$,

$$I^{(m)} \simeq \int_a^\infty dr r^{1-\alpha m} = \frac{a^{2-m\alpha}}{m\alpha - 2} \xrightarrow{\alpha \rightarrow 2} \begin{cases} \sim \frac{1}{\alpha-2} & : m = 1, \\ \text{const.} & : m > 1. \end{cases} \quad (38)$$

For $\alpha \rightarrow 2$ from above, $I^{(m)}$ only diverges for $m = 1$ whereas it is finite for $m > 1$.

From Eq. (37) the MF critical temperature is

$$T_c^{(0)} = |J_1| b_{c,1} I^{(1)} \sim \frac{1}{\alpha - 2}, \quad (39)$$

see the green line in Fig. 5. We thus use $\alpha - 2$ as the small parameter for the expansion on the right-hand side of Eq. (37). We consider the geometry factors $\beta^n t_{\mathbf{k}=0}^{(nx)}$ that play a role for the static Heisenberg case and we limit ourselves to order $n \leq 3$. For diagram (3b), we numerically checked that $\sum_{i,j} J_{r_j} J_{r_i - r_j} J_{r_i} \equiv J_1^3 \tilde{I}^{(3)}$ is nonsingular for $\alpha \rightarrow 2$. In summary, this means that $T \Sigma^{(n)} \sim \beta^n \sim [\alpha - 2]^n$ around criticality. We expand the right-hand side in Eq. (37) to third order in $\alpha - 2$ and obtain

$$\begin{aligned} b_{c,1} \beta |J_1| I^{(1)} &= 1 - b_{c,1}^{-1} (\beta |J_1|)^2 I^{(2)} T^3 (\sigma^{(2a)} + \sigma^{(2b)}) \\ &\quad + b_{c,1}^{-1} (\beta |J_1|)^3 T^4 [I^{(3)} (\sigma^{(3a)} + \sigma^{(3c)}) \\ &\quad + \tilde{I}^{(3)} \sigma^{(3b)}] + \dots \end{aligned} \quad (40)$$

The results for $S = 1/2$ are shown in Fig. 5 and approach the QMC data quickly if $\alpha - 2$ is sufficiently small.

B. Dicke-Ising model: Ground-state superradiance

As a second application to a many-body quantum optical system we consider the Dicke-Ising model [43,44,61,62]. This also provides an example where single-spin blocks appear in the diagrammatic expansion. This means that the precom-

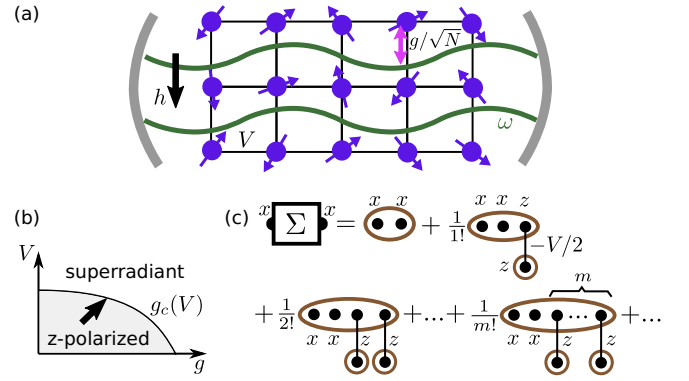


FIG. 6. Dicke-Ising model: (a) Sketch of an experimental square lattice setup with cavity photons at frequency ω coupled to spins with strength g/\sqrt{N} , homogeneous z field h and nearest-neighbor AFM Ising interactions V induced via Rydberg dressing. (b) Schematic phase diagram in the vicinity of the z -polarized phase and the adjacent superradiant phase in the presence of AFM Ising interactions V . (c) The diagrammatic expansion for Σ^{xx} in the limit $N \rightarrow \infty$ and $T \rightarrow 0$ can be summed exactly. This shows that the exact phase boundary in (b) is described by the MF result Eq. (45).

puted diagrams of Sec. III cannot be used in the following calculation, see below.

The Hamiltonian features a competition between a homogeneous field $h > 0$ in z direction, a coupling of the total spin x to a cavity photon and a nearest-neighbor AFM Ising zz interaction V , see Fig. 6(a) for a sketch. For concreteness, we specialize to a square lattice geometry. However, our qualitative results below do not depend on this choice. The Hamiltonian is $H = H_x + H_z$ with

$$H_x = \omega a^\dagger a + \frac{g}{\sqrt{N}} (a + a^\dagger) \sum_i S_i^x, \quad (41)$$

$$H_z = -h \sum_i S_i^z + \frac{V}{2} \sum_{(i,i')} \left(S_i^z + \frac{1}{2} \right) \left(S_{i'}^z + \frac{1}{2} \right) \quad (42)$$

$$= -[h - V] \sum_i S_i^z + \frac{V}{2} \sum_{(i,i')} S_i^z S_{i'}^z. \quad (43)$$

Here, the cavity photon at frequency ω is created by a^\dagger . The sums go over N sites and the nearest-neighbor bonds, respectively. The cavity-dipole coupling is $g/\sqrt{N} > 0$. This ensures an extensive interacting energy in the infinite system limit $N \rightarrow \infty$, which we consider in the following.

The Dicke model (the case $V = 0$) and its phase transition to the symmetry-broken superradiant state (the FM state with $\langle S_i^x \rangle \neq 0$) has been studied thoroughly both in theory [17,32] and experiment [6], the latter in a nonequilibrium setting. However, comparatively little is known about the Dicke-Ising model ($V > 0$) [43,44,61,62], which is yet awaiting experimental implementation. A possible realization for the Ising zz interactions uses the concept of Rydberg dressing [63], which motivated the form of Eq. (42) and leads to a renormalized effective field $h \rightarrow h - V$ when rewritten as in Eq. (43).

So far, the model also contains bosonic degrees of freedom in variance to the spin-only formulation in Hamiltonian (1). However, assuming a thermal state we can trace out the photons on the level of the generating functional [64]. This

replaces H_x by an all-to-all retarded (i.e., frequency-dependent) FM spin interaction of the xx type,

$$H_x \rightarrow H_{x,\text{ret}} = T \sum_{\nu_m} \frac{1}{2} \sum_{i,i'} S_i^x(-\nu_m) J_{ii'}^{xx}(\nu_m) S_{i'}^x(\nu_m), \quad (44)$$

with $J_{ii'}^{xx}(\nu_m) = -2g^2\omega/[N(\nu_m^2 + \omega^2)]$. This is close to Eq. (1), only differing in the frequency dependence and the presence of an on-site term. As we will discuss, this is inconsequential in the following since no xx interactions will appear in the 1J diagrammatic expansion.

Here, we focus on thermal equilibrium at $T \rightarrow 0$ and limit the investigation to the realistic case of small V ($V \ll h$) and its effect on the transition between the z -polarized and superradiant phase. For $V \rightarrow 0$, it is well known that the MF approximation is exact for the Dicke model [17] but what happens at $V > 0$? As a first step, in Ref. [43] the phase boundary for the Dicke-Ising model on the square lattice was determined in MF approximation,

$$g_c = \sqrt{\omega(h - 2V)}, \quad (45)$$

see Fig. 6(b) for a sketch.

Two questions are in order: First, is the phase transition indeed continuous as in MF approximation? And second, if yes, what are the corrections to the phase boundary beyond the MF prediction?

As shown in Ref. [62] for a simplified and more symmetric version of the Dicke-Ising model with $h - V = 0$ (with no z -polarized phase), the transition between the superradiant and Ising phase is of first order in a chain geometry. However, it is currently unknown if and under which conditions this also holds for the case $V \ll h$ and the phase transition out of the fully polarized phase that we consider.

Making the assumption that the phase transition from the z -polarized to the superradiant phase is continuous (and can thus be detected via a divergence in spin susceptibility) we use the spin diagrammatic technique to show rigorously our main finding of this section: Eq. (45) is already the exact result. This conclusion has been obtained independently in the very recent work of Schellenberger and Schmidt [44] using an alternative algebraic approach.

Analogous to the other examples in this work, we start from the z -polarized symmetry-unbroken phase and approach the boundary of the superradiant phase, see the arrow in Fig. 6(b). We detect the critical light-matter coupling strength g_c from the divergence of the static FM correlator $G_{\mathbf{k}=0}^{xx}(i\nu = 0)$,

$$1/\Sigma_{\mathbf{k}=0}^{xx} + J_{\mathbf{k}=0}^{xx} \stackrel{!}{=} 0. \quad (46)$$

Here and in the following we drop the zero-Matsubara frequency argument from all quantities. The static part of the retarded xx interaction (44) is $J_{\mathbf{k}=0}^{xx} = -2g^2/(\omega N)$ and Σ^{xx} denotes the J^{xx} -irreducible part of G^{xx} . Next, we expand Σ^{xx} in J^{xx} and V with the noninteracting Hamiltonian being $H_{0,h-V} = -[h - V] \sum_i S_i^z$. The first observation is that due to the limit $N \rightarrow \infty$ any occurrence of an interaction $J_{ii'}^{xx} \sim 1/N$ needs to be accompanied with a free site summation. Since these diagrams are necessarily J^{xx} -reducible (cf. the discussion at the end of Sec. II B) they do not occur in Σ^{xx} and only the V interactions $\sim S_i^z S_{i'}^z$ need to be considered. The second observation pertains to z -only blocks $G_{0,c,h-V}^{z,\dots,z}(\tau_1, \dots, \tau_m) =$

$b_c^{(m-1)}(\beta[h - V])$. In the limit $T \rightarrow 0$ where the spins are fully polarized, these generalized susceptibilities vanish except for $m = 1$ for which $G_{0,c,h-V}^z(\tau_1) = S = 1/2$.

These considerations equate the exact (and local) Σ^{xx} to the infinite sum of diagrams shown in Fig. 6(c). The calculation proceeds without the kernel trick since all diagrammatic objects are free of frequency loops and are easily evaluated at the required zero frequency. We only need $\Sigma^{xx(0)} = 1/(2[h - V])$, see Table II for the TFIM. The fully static mixed-flavor blocks with two S^x operators and m appearances of the S^z operator can be found via a m -fold derivative of $G_{0,c,h-V}^{xx}$ with respect to h (which thus is also used as a source field),

$$G_{0,c,h-V}^{\overbrace{xxz \dots z}^m} = \partial_h^m G_{0,c,h-V}^{xx} = \frac{(-1)^m m!}{2[h - V]^{m+1}}. \quad (47)$$

With these preparations the infinite diagrammatic sum in Fig. 6(c) results in the exact expression

$$\begin{aligned} \Sigma_{\mathbf{k}=0}^{xx} &= \sum_{m=0}^{\infty} \frac{1}{m!} G_{0,c,h-V}^{\overbrace{xxz \dots z}^m} \cdot \langle S^z \rangle_{0,c}^m \cdot \left(-4\frac{V}{2}\right)^m \\ &= \frac{1}{2(h - 2V)}. \end{aligned} \quad (48)$$

Inserting this in Eq. (46) we obtain that the exact g_c is already given by Eq. (45).

For future work on the Dicke-Ising model, an extension to the complete phase diagram, which includes also a z -AFM and a combined z -AFM and superradiant x -FM phase, would be interesting. According to Ref. [44], MF theory is again exact for the transition between the latter two phases. Likewise, we suggest to consider the experimentally relevant modifications to finite N and the open-system case [65].

VI. CONCLUSION

In summary, we have presented an analytic approach to Matsubara spin-spin correlation functions based on a diagrammatic expansion of their 1- J -irreducible part Σ to n th order in J . We provide closed-form expressions for $n \leq 4$ for Ising, TFIM and Heisenberg models of completely general lattice geometry and spin length S . The introduction of the kernel function trick was instrumental in this calculation. The final results are conveniently tabulated for forthcoming application in diverse contexts where other computationally much more involved methods such as tensor networks or QMC are at their limits.

Via many examples and by applying a composite expansion strategy involving the inverse spatial dimension (or similar) as a small parameter, we showed the quantitative success of the diagrammatic approach if applied to models qualitatively described by the MF approximation. We argued that this is often the case in highly connected spin models relevant for state-of-the-art many-body quantum optical experiments. We use a long-range Heisenberg model and the Dicke-Ising model, both on the square lattice, as a showcase. Moreover we provided various benchmark examples for nearest-neighbor models on the (hyper)cubic lattice where our method yields accurate magnetic phase boundaries (both at $T > 0$ for Ising and Heisenberg models and $T = 0$ for

TFIM). We emphasize that due to the analytic nature of our approach, continuation to real frequencies is easily performed. For example we showed competitive results for the gap in the TFIM.

Future work could extend our approach to yet higher orders in J (for which diagram creation can be automated) or a greater variety of spin models, including those with non-trivial unit cells or various forms of disorder. Also spin-spin couplings between sites i, i' that are characterized by two or more nonzero parameters in the 3×3 coupling matrix $J_{ii'}^{\gamma\gamma'}$ [cf. Eq. (1)], e.g., XXZ models [66] could be studied with little extra effort. Another option would be to extend our approach to systems with $SU(N)$ symmetry for $N > 2$ [67,68]. Also, the treatment of the symmetry-broken phase for the study of magnetization and spin-wave properties [48,69] is within reach. Further, it would be interesting to consider analytic continuation beyond the computation of the gap to obtain spectral functions. These are routinely measured in inelastic neutron scattering on solid-state magnets [70] or, more recently via quench spectroscopy in Rydberg tweezer arrays [23]. For the static case, analytic insights offered by our approach proved essential to shed new light [71] onto the puzzle of quantum-to-classical correspondence for static spin correlation functions in $d > 1$ dimensions [72].

Finally, we point out that the combination of the spin-spin correlator's bare series expansion with the kernel function trick [cf. Eq. (B2)] is suitable for evaluation by a diagrammatic Monte Carlo approach [73] similar to the connected determinant method [47]. However, imaginary time integrals are treated exactly via the kernel functions. Implementing these ideas would enhance the available expansion orders in spin diagrammatics and allow for flexible resummation schemes beyond this work.

Note added. Recently, we became aware of independent work in Ref. [74], which computes $\Sigma^{(0,2,3)}$ for the Heisenberg model in the traditional diagrammatic way via frequency integrals. The diagrams were derived from an expansion of spin-IRG flow equations and the five-point free spin correlator was provided analytically. Applications concern the chiral nonlinear susceptibility and estimates of T_c for the $d = 3, 4$ hypercubic case for various S . However, due to the chosen expansion of $1/\Sigma$ in J , the quality of the results for T_c does not improve with expansion order, in contrast to the composite expansion strategies presented in this work.

ACKNOWLEDGMENTS

We thank Marin Bukov, Elio König, Peter Kopietz, Andreas Rückriegel, Achim Rosch, Johannes Reuther, Kai Schmidt, Nils Schopohl, and Sebastian Slama for useful discussions and the authors of Ref. [59] for sharing their iPEPS data. We acknowledge funding from the Deutsche Forschungsgemeinschaft (DFG, German Research Foundation) through the Research Unit FOR 5413/1, Grant No. 465199066. B.Sch. acknowledges funding from the Munich Quantum Valley, supported by the Bavarian state government with funds from the Hightech Agenda Bayern Plus. B.Sb. and B. Schneider are supported by DFG Grant No. 524270816. I.L. acknowledges financing from the Baden-Württemberg Stiftung through Project No. BWST_ISF2019-23.

APPENDIX A: V -CONNECTED CORRELATORS

We define the V -connected correlators [47] (subscript $V - c$) that appear in the formal expansion of the spin correlator in Eq. (11) and the following equations. For brevity, we set $S_j^{\gamma'}(\tau)S_j^{\gamma}(\tau') = A$. Then the V -connected correlators are defined recursively via

$$\begin{aligned} \langle \mathcal{T}V(\tau_1) \dots V(\tau_n)A \rangle_{0,h,V-c} &= \langle \mathcal{T}V(\tau_1) \dots V(\tau_n)A \rangle_{0,h} \\ &- \sum_{S \subseteq \{1, \dots, n\}} \left\langle \mathcal{T} \prod_{j \in S} V(\tau_j)A \right\rangle_{0,h,V-c} \left\langle \mathcal{T} \prod_{k \in \{1, \dots, n\} \setminus S} V(\tau_k) \right\rangle_{0,h}. \end{aligned} \quad (\text{A1})$$

Note that the ordering of (bosonic) operators behind imaginary time-ordering operator \mathcal{T} does not matter. Standard connected spin correlators [with subscript c first appearing in Eq. (13)] are defined in analogy to their V -connected counterparts in Eq. (A1) by replacing each $V(\tau_j)$ with a single spin operator and removing the external operators $A \rightarrow 1$.

APPENDIX B: EVALUATION OF $\sigma^{\gamma\gamma'(nx)}(iv_m)$ VIA KERNEL FUNCTION TRICK

To facilitate all calculations on the right-hand side of Eq. (12) and in particular the evaluation of $\sigma^{(nx)}$ we introduce what we call the kernel function trick. Originally, kernel functions have been introduced to link the Fourier transform of an imaginary time-ordered m -point correlation function $G_{A_1 \dots A_m}(i\omega_1, \dots, i\omega_{m-1})$ to eigenstates and -energies $H|a\rangle = E_a|a\rangle$ of the many-body Hamiltonian [75]. The m -point correlators are a generalization of Eq. (7) to m arbitrary operators $A_{1,2,\dots,m}$. For the frequency arguments we introduced an abbreviated notation where ω_1 is short for ω_{n_1} and so on. The kernel functions straightforwardly extend the well-known spectral (or Lehmann) representation of the two-point correlator [27] to the m -point case. For bosonic (and spin) operators, the Fourier transform reads [49]

$$\begin{aligned} G_{A_1 \dots A_m}(i\omega_1, \dots, i\omega_{m-1}) &= \frac{1}{Z} \sum_{p \in S_m} \sum_{\underline{1} \dots \underline{m}} e^{-\beta E_{\underline{1}}} A_{p(1)}^{12} A_{p(2)}^{23} \dots A_{p(m)}^{m1} K_m \\ &\times (\Omega_{p(1)}^{12}, \Omega_{p(2)}^{23}, \dots, \Omega_{p(m-1)}^{m-1m}), \end{aligned} \quad (\text{B1})$$

where $A_k^{ab} = \langle a|A_k|b\rangle$ are matrix elements and the argument of the kernel function K_m is a list of m complex numbers $\Omega_k^{ab} \equiv i\omega_k + E_a - E_b$, which sum to zero so that the last one is often dropped as in Eq. (B1). The kernel function itself are completely universal and do neither depend on the Hamiltonian H nor on the operators A_k in Eq. (B1). For example, $K_2(\Omega_1) = -\Delta_{\Omega_1} + \beta\delta_{\Omega_1}/2$ where $\delta_x = \delta_{0,x}$ and $\Delta_x = (1 - \delta_x)/x$. The recent advance in Ref. [49] was the calculation of K_m for general m .

In the context of diagram evaluation, the crucial insight is that Eq. (B1) and n th-order perturbative expressions are naturally connected by interpreting the right-hand side of Eq. (12) as a Fourier transform of a time-ordered correlator of order $n + 2$ with the first n frequencies being zero. Hence, as the

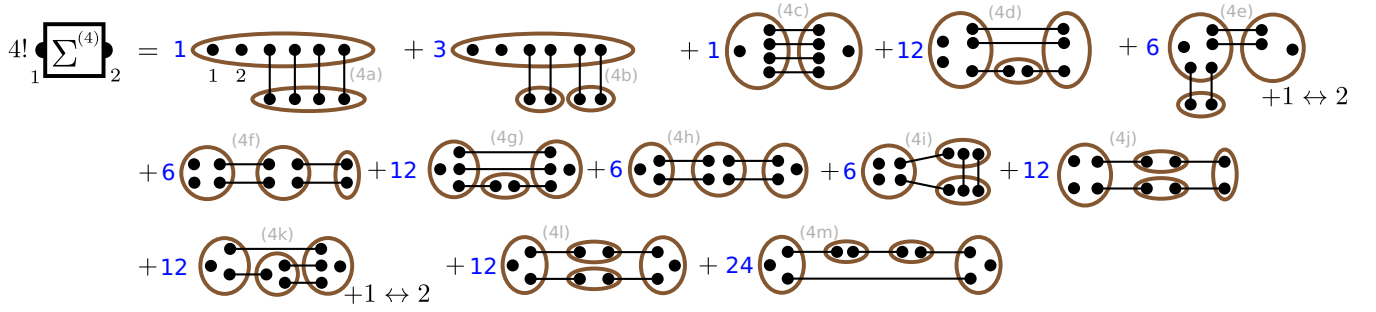


FIG. 7. Diagrams for Σ of order J^4 , analogous to Fig. 3. The label $+1 \leftrightarrow 2$ adds the diagram with exchanged external indices.

main technical result of this work, Eq. (12) is expressed as

$$G_{jj'}^{\gamma\gamma'(n)}(iv_m) = \frac{(-1)^n}{n!} \sum_{p \in \mathcal{S}_{n+2}} \sum_{i_1 < i'_1, \dots, i_n < i'_n} \sum_{\gamma_1, \dots, \gamma_n \in \{+, -, z\}} J_{i_1 i'_1}^{\gamma_1 \gamma'_1} \dots J_{i_n i'_n}^{\gamma_n \gamma'_n} \langle B_{p(1)} B_{p(2)} \dots B_{p(n+2)} \rangle_{0, h, V-c} K_{n+2}(\Omega_{p(1)}, \Omega_{p(2)}, \dots, \Omega_{p(n+1)}). \quad (\text{B2})$$

Here we replaced V using Eq. (10) and defined the following operator and complex-frequency lists

$$\{B_1, \dots, B_n, B_{n+1}, B_{n+2}\} = \{S_{i_1}^{\gamma_1} S_{i'_1}^{\gamma'_1}, \dots, S_{i_n}^{\gamma_n} S_{i'_n}^{\gamma'_n}, S_j^{\gamma_j}, S_{j'}^{\gamma'_j}\}, \quad (\text{B3})$$

$$\{\Omega_1, \dots, \Omega_n, \Omega_{n+1}, \Omega_{n+2}\} = \{-(\gamma_1 + \gamma'_1)h, \dots, -(\gamma_n + \gamma'_n)h, iv_m - \gamma h, -iv_m - \gamma' h\}. \quad (\text{B4})$$

Note that the external indices on the left-hand side of Eq. (B2) determine the last two entries of the lists. The Ω list (B4) was already given in Eq. (23). It is to be understood with the following replacement rule of flavor labels by numbers: $\{z, +, -\} \rightarrow \{0, +1, -1\}$. The simple structure of $H_{0,h}$ with its many-body (product) eigenstates and ladderlike energies is essential in the derivation of Eq. (B2) as it allows to reduce the complexity of the general Eq. (B1) by rewriting the sum over eigenstates via the equal-time free spin correlator. The point is that the $\Omega_k^{ab} \equiv i\omega_k + E_a - E_b$ only depend on the flavor(s) $\{+, -, z\}$ of the (composite) operator B_k .

Further, we rewrite Eq. (B2) using an index ordering operator \mathcal{P} . This operator applies to operator strings and argument lists alike. It acts like time-ordering, but for discrete indices $(1), (2), \dots, (n+2)$ that, unlike imaginary time arguments, do not affect the operator, for example $\mathcal{P}B_1(1)B_2(3)B_3(2) = B_2B_3B_1$. We also reinstate the redundant last argument $\Omega_{p(n+2)}$ of K_{n+2} . We obtain

$$G_{jj'}^{\gamma\gamma'(n)}(iv_m) = \frac{(-1)^n}{n!} \sum_{p \in \mathcal{S}_{n+2}} \sum_{i_1 < i'_1, \dots, i_n < i'_n} \sum_{\gamma_1, \dots, \gamma_n \in \{+, -, z\}} J_{i_1 i'_1}^{\gamma_1 \gamma'_1} \dots J_{i_n i'_n}^{\gamma_n \gamma'_n} \times \langle \mathcal{P}B_1(p_1)B_2(p_2) \dots B_{n+2}(p_{n+2}) \rangle_{0, h, V-c} K_{n+2}(\mathcal{P}\{\Omega_1(p_1), \Omega_2(p_2), \dots, \Omega_{n+2}(p_{n+2})\}), \quad (\text{B5})$$

As the operators B_1, B_2, \dots, B_{n+2} and their associated $\Omega_1, \Omega_2, \dots, \Omega_{n+2}$ appear in all possible orderings, this is evidently the same as Eq. (B2).

To calculate $\sigma^{\gamma\gamma'(nx)}(iv_m)$ for a particular 1JI diagram (nx) defined by reference site configuration $\{i_k^{(nx)} < i'_k^{(nx)}\}_{k=1,2,\dots,n}$, we specialize the site sums in Eq. (B5) to this reference configuration and split off the geometry factor $t^{(nx)}[J]$ as explained in Sec. II C. The V -connected average then becomes an ordinary connected equal-time average with respect to $H_{0,h}$, which factorizes according to the blocks of equal sites characteristic for (nx) . Examples for diagrams (2a) and (3b) are provided in Eqs. (21) and (22), respectively.

APPENDIX C: SIMPLIFIED KERNEL FUNCTIONS FOR THE SPECIAL CASES $h = 0$ AND $T = 0$

Kernel functions $K_k(\Omega_1, \Omega_2, \dots, \Omega_k)$ for general complex arguments (obeying $\Omega_1 + \dots + \Omega_k = 0$) and arbitrary $k = 2, 3, 4, 5, 6, \dots$ are provided in Ref. [49]. However, in the context of this paper, where kernel functions are applied in the framework of spin perturbation theory, we have only two potentially nonreal entries in the Ω list (B4) (the ones at the end, which contain $\pm iv_m$ related to the external operators). More importantly, we limit ourselves to two special cases, (i) the case $h = 0$ for the Ising and Heisenberg model and (ii) the limit $T \rightarrow 0$ for the TFIM. In these cases substantial simplifications arise.

(i) Case $h = 0$: In Eq. (B5), the arguments of K_k are zero except for a possible nonzero pair of frequencies $\pm iv_m = \pm 2m\pi T i$ shuffled to positions $a_{1,2}$ in the list of length $k = n + 2$,

$$\{\Omega_1, \Omega_2, \dots, \Omega_k\} = (0, 0, \dots, 0, \underbrace{iv_m}_{\text{pos. } a_1}, 0, \dots, 0, \underbrace{-iv_m}_{\text{pos. } a_2}, \underbrace{0, \dots, 0}_{k-a_2}), \quad (\text{C1})$$

TABLE VI. Geometry factors $t^{(nx)}[J]$ for Σ diagrams of order $n = 4$. See the caption of Table I for remarks.

| top. | r space $t_{jj'}^{(nx)}$ | k space $t_{\mathbf{k}}^{(nx)}$ | nn-hyp. $\tilde{t}_{\mathbf{k}}^{(nx)}$ |
|------|--|--|--|
| (4a) | $\delta_{jj'} \sum_i J_{ij}^4$ | $\int_{\mathbf{p}_{1,2,3}} J_{\mathbf{p}_1} J_{\mathbf{p}_2} J_{\mathbf{p}_3} J_{\mathbf{p}_1+\mathbf{p}_2+\mathbf{p}_3}$ | $J_1^3 \tilde{J}_0$ |
| (4b) | $\delta_{jj'} [\sum_i J_{ji}^2]^2$ | $[\int_{\mathbf{q}} J_{\mathbf{q}}^2]^2$ | $[J_1 \tilde{J}_0]^2$ |
| (4c) | $J_{jj'}^4$ | $\int_{\mathbf{p}_{1,2,3}} J_{\mathbf{k}-\mathbf{p}_1} J_{\mathbf{p}_2} J_{\mathbf{p}_3} J_{\mathbf{p}_1+\mathbf{p}_2+\mathbf{p}_3}$ | $J_1^3 \tilde{J}_{\mathbf{k}}$ |
| (4d) | $\delta_{jj'} \sum_i J_{ji}^2 [J \cdot J]_{ij}$ | $\int_{\mathbf{q}, \mathbf{p}} J_{\mathbf{q}} J_{\mathbf{p}} J_{\mathbf{q}+\mathbf{p}}^2$ | 0 |
| (4e) | $J_{jj'}^2 \sum_i [J_{ji}^2 + J_{ji'}^2]$ | $2[\int_{\mathbf{p}} J_{\mathbf{p}}^2][\int_{\mathbf{q}} J_{\mathbf{k}-\mathbf{q}} J_{\mathbf{q}}]$ | $2J_1^2 \tilde{J}_0 \tilde{J}_{\mathbf{k}}$ |
| (4f) | $\delta_{jj'} \sum_{i_1, i_2} J_{ji_1}^2 J_{ji_2}^2$ | $[\int_{\mathbf{q}} J_{\mathbf{q}}^2]^2$ | $[J_1 \tilde{J}_0]^2$ |
| (4g) | $J_{jj'}^2 [J \cdot J]_{jj'}$ | $\int_{\mathbf{q}, \mathbf{p}} J_{\mathbf{k}-\mathbf{p}} J_{\mathbf{p}-\mathbf{q}} J_{\mathbf{q}}^2$ | 0 |
| (4h) | $[J^2 \cdot J^2]_{jj'}$ | $[\int_{\mathbf{q}} J_{\mathbf{k}-\mathbf{q}} J_{\mathbf{q}}]^2$ | $[J_1 \tilde{J}_{\mathbf{k}}]^2$ |
| (4i) | $\delta_{jj'} [J \cdot J^2 \cdot J]_{jj}$ | $\int_{\mathbf{q}} \int_{\mathbf{p}} J_{\mathbf{q}} J_{\mathbf{p}} J_{\mathbf{q}+\mathbf{p}}^2$ | 0 |
| (4j) | $\delta_{jj'} [J \cdot J \cdot J \cdot J]_{jj}$ | $\int_{\mathbf{q}} J_{\mathbf{q}}^4$ | $6d[2d-1]J_1^4$ |
| (4k) | $J_{jj'} [J \cdot J^2 + J^2 \cdot J]_{jj'}$ | $2 \int_{\mathbf{q}} J_{\mathbf{k}-\mathbf{q}} J_{\mathbf{q}} \int_{\mathbf{p}} J_{\mathbf{p}-\mathbf{q}} J_{\mathbf{p}}$ | 0 |
| (4l) | $[J \cdot J]_{jj'}$ | $\int_{\mathbf{q}} J_{\mathbf{k}-\mathbf{q}}^2 J_{\mathbf{q}}^2$ | $16J_1^4 (\frac{d^2}{4} + \frac{1}{8} \sum_{\mu=1}^d \cos(2k_{\mu}) + \sum_{\mu < \nu}^d \cos k_{\mu} \cos k_{\nu})$ |
| (4m) | $J_{jj'} [J \cdot J \cdot J]_{jj'}$ | $\int_{\mathbf{q}} J_{\mathbf{k}-\mathbf{q}} J_{\mathbf{q}}^3$ | $3[2d-1]J_1^3 \tilde{J}_{\mathbf{k}}$ |

where we assume $a_1 < a_2$ without loss of generality (see below). For this situation, we define

$$K_k(\Omega_1, \Omega_2, \dots, \Omega_k) \equiv K_k^{(h=0)}(a_1, a_2, m). \quad (C2)$$

From Ref. [49], we find after some algebra

$$T^{k-1} K_k^{(h=0)}(a_1, a_2, m) = \begin{cases} \frac{1}{k!} & : m = 0, \\ (-1)^{a_2-a_1} \sum_{l=a_2-a_1}^{k-a_1} \frac{[\Delta_{2\pi m l}]!}{(k-l)!} \binom{l-1}{a_2-a_1-1} & : \text{otherwise,} \end{cases} \quad (C3)$$

where $\Delta_x = 1/x$ for nonzero x and zero otherwise. For the case that $-iv_m$ appears first, $a_1 > a_2$, we can flip the sign of m and obtain $K_k(\Omega_1, \Omega_2, \dots, \Omega_k) = K_k^{(h=0)}(a_2, a_1, -m)$.

(ii) Case $T \rightarrow 0$: Here the kernel functions simplify because certain sums are dominated by inverse temperature $\beta \rightarrow \infty$. Any $\beta \delta_{\omega_1+\dots+\omega_l, 0}$ that remains must be interpreted as $\beta \delta_{\omega_1+\dots+\omega_l, 0} \xrightarrow{T \rightarrow 0} 2\pi \delta(\omega_1 + \dots + \omega_l)$, but this does not appear for the particular

 TABLE VII. Ising model, TFIM at $T = 0$ and Heisenberg model: The lattice independent part $\sigma^{(nx)}$ for $n = 4$ for all topologies, cf. Eq. (18). The Ising case is purely static.

| | Ising $T^{1+n} \sigma^{zz(nx)}$ | TFIM $\sigma^{xx(nx)}(iv) _{T=0}$ | Heisenberg: $T^{1+n} \sigma^{zz(nx)}(0)$ | Heisenberg: $T^{1+n} \sigma^{zz(nx)}(iv_m \neq 0)$ |
|------|-----------------------------------|---|---|--|
| (4a) | $\frac{1}{4!} b_{c,3} b_{c,5}$ | $\frac{-S^2(195h^4+38h^2v^2+3v^4)}{512h^3(h^2+v^2)^2(9h^2+v^2)}$ | $\frac{b_{c,1}^2}{-240} (192b_{c,1}^3 + 80b_{c,1}^2 + 20b_{c,1} + 3)$ | $\frac{\Delta^2 b_{c,1}^2}{15} (4[30\Delta^2 + 1]b_{c,1} + 12b_{c,1}^2 + 15\Delta^2 + 2)$ |
| (4b) | $\frac{3}{4!} b_{c,1}^3 b_{c,5}$ | $\frac{S^3(447h^6+405h^4v^2+93h^2v^4+7v^6)}{256h^3(h^2+v^2)^3(9h^2+v^2)}$ | $\frac{b_{c,1}^3}{24} (48b_{c,1}^2 + 12b_{c,1} + 1)$ | $\frac{\Delta^2 b_{c,1}^3}{-3} (6b_{c,1} + 30\Delta^2 + 1)$ |
| (4c) | 0 | 0 | $\frac{b_{c,1}^2}{-120} (12b_{c,1}^2 + 6b_{c,1} + 1)$ | $\frac{\Delta^2 b_{c,1}^2}{-15} (4[30\Delta^2 + 1]b_{c,1} + 12b_{c,1}^2 + 15\Delta^2 + 2)$ |
| (4d) | 0 | 0 | $\frac{b_{c,1}^3}{24} (4b_{c,1} + 1)$ | $\frac{\Delta^2 b_{c,1}^3}{-2}$ |
| (4e) | 0 | 0 | $\frac{b_{c,1}^3}{48} (4b_{c,1} + 1)$ | $\frac{\Delta^2 b_{c,1}^3}{3} (6b_{c,1} + 30\Delta^2 + 1)$ |
| (4f) | $\frac{6}{4!} b_{c,1} b_{c,3}^2$ | $\frac{S^3(21h^2+5v^2)}{256h^3(h^2+v^2)^2}$ | $b_{c,1}^3 (b_{c,1}^2 + \frac{b_{c,1}}{3} + \frac{1}{30})$ | $\frac{\Delta^2 b_{c,1}^3}{-3} (6b_{c,1} + 12\Delta^2 + 1)$ |
| (4g) | $\frac{12}{4!} b_{c,1} b_{c,3}^2$ | $\frac{S^3(21h^2+v^2)}{16h(h^2+v^2)^2(9h^2+v^2)}$ | $\frac{b_{c,1}^3}{120} (144b_{c,1}^2 + 48b_{c,1} + 5)$ | $\frac{b_{c,1}^3}{3} \Delta^2 (12\Delta^2 + 1)$ |
| (4h) | 0 | 0 | $\frac{b_{c,1}^3}{120}$ | $-6\Delta^2 b_{c,1}^3$ |
| (4i) | 0 | 0 | $\frac{b_{c,1}^3}{120} (10b_{c,1} + 1)$ | $\frac{b_{c,1}^3}{6} \Delta^2 (24\Delta^2 - 1)$ |
| (4j) | $\frac{12}{4!} b_{c,1}^3 b_{c,3}$ | $\frac{-5S^4(11h^2+3v^2)}{256h^3(h^2+v^2)^2}$ | $\frac{b_{c,1}^4}{-6} (6b_{c,1} + 1)$ | $+2\Delta^2 b_{c,1}^4$ |
| (4k) | 0 | 0 | $\frac{b_{c,1}^3}{-120}$ | $\frac{b_{c,1}^3}{-6} \Delta^2 (24\Delta^2 - 1)$ |
| (4l) | 0 | 0 | 0 | 0 |
| (4m) | 0 | 0 | 0 | $-2\Delta^2 b_{c,1}^4$ |

correlators we compute in this work. To express the resulting $K_k^{(T \rightarrow 0)}(\Omega_1, \dots, \Omega_k)$ we define the list of the partial sums

$$\{\Omega_1, \Omega_1 + \Omega_2, \Omega_1 + \Omega_2 + \Omega_3, \dots, \Omega_1 + \dots + \Omega_{k-1}\} \equiv \{c_1, c_2, \dots, c_{k-1}\}. \quad (\text{C4})$$

The final expression for $K_k^{(T \rightarrow 0)}$ involves a product of all but the l entries of (C4), which are zero,

$$K_k^{(T \rightarrow 0)}(\Omega_1, \dots, \Omega_k) = (-1)^{k+1+l} \frac{\beta^l}{(l+1)!} \prod_{c_m \neq 0} \frac{1}{c_m}. \quad (\text{C5})$$

APPENDIX D: DIAGRAMS AND RESULTS FOR $\Sigma^{(4)}$

In Fig. 7 we provide the diagrams for Σ to order J^4 with geometry factors and $\sigma^{(nx)}$ given in Tables VI and VII.

-
- [1] M. Endres, H. Bernien, A. Keesling, H. Levine, E. R. Anschuetz, A. Krajenbrink, C. Senko, V. Vuletic, M. Greiner, and M. D. Lukin, Atom-by-atom assembly of defect-free one-dimensional cold atom arrays, *Science* **354**, 1024 (2016).
- [2] D. Barredo, S. de Léséleuc, V. Lienhard, T. Lahaye, and A. Browaeys, An atom-by-atom assembler of defect-free arbitrary two-dimensional atomic arrays, *Science* **354**, 1021 (2016).
- [3] J. T. Barreiro, M. Müller, P. Schindler, D. Nigg, T. Monz, M. Chwalla, M. Hennrich, C. F. Roos, P. Zoller, and R. Blatt, An open-system quantum simulator with trapped ions, *Nature (London)* **470**, 486 (2011).
- [4] A. Shankar, E. A. Yuzbashyan, V. Gurarie, P. Zoller, J. J. Bollinger, and A. M. Rey, Simulating dynamical phases of chiral $p + ip$ superconductors with a trapped ion magnet, *PRX Quantum* **3**, 040324 (2022).
- [5] A. Frisk Kockum, A. Miranowicz, S. De Liberato, S. Savasta, and F. Nori, Ultrastrong coupling between light and matter, *Nature Rev. Phys.* **1**, 19 (2019).
- [6] K. Baumann, C. Guerlin, F. Brennecke, and T. Esslinger, Dicke quantum phase transition with a superfluid gas in an optical cavity, *Nature (London)* **464**, 1301 (2010).
- [7] R. Landig, L. Hruby, N. Dogra, M. Landini, R. Mottl, T. Donner, and T. Esslinger, Quantum phases from competing short- and long-range interactions in an optical lattice, *Nature (London)* **532**, 476 (2016).
- [8] A. Browaeys and T. Lahaye, Many-body physics with individually-controlled Rydberg atoms, *Nature Phys.* **16**, 132 (2020).
- [9] C. Monroe, W. C. Campbell, L.-M. Duan, Z.-X. Gong, A. V. Gorshkov, P. W. Hess, R. Islam, K. Kim, N. M. Linke, G. Pagano, P. Richerme, C. Senko, and N. Y. Yao, Programmable quantum simulations of spin systems with trapped ions, *Rev. Mod. Phys.* **93**, 025001 (2021).
- [10] S.-A. Guo, Y.-K. Wu, J. Ye, L. Zhang, W.-Q. Lian, R. Yao, Y. Wang, R.-Y. Yan, Y.-J. Yi, Y.-L. Xu, B.-W. Li, Y.-H. Hou, Y.-Z. Xu, W.-X. Guo, C. Zhang, B.-X. Qi, Z.-C. Zhou, L. He, and L.-M. Duan, A site-resolved two-dimensional quantum simulator with hundreds of trapped ions, *Nature (London)* **630**, 613 (2024).
- [11] W. Guerin, M. O. Araújo, and R. Kaiser, Subradiance in a large cloud of cold atoms, *Phys. Rev. Lett.* **116**, 083601 (2016).
- [12] J. Rui, D. Wei, A. Rubio-Abadal, S. Hollerith, J. Zeiher, D. M. Stamper-Kurn, C. Gross, and I. Bloch, A subradiant optical mirror formed by a single structured atomic layer, *Nature (London)* **583**, 369 (2020).
- [13] P. Kongkhambut, J. Skulte, L. Mathey, J. G. Cosme, A. Hemmerich, and H. Keßler, Observation of a continuous time crystal, *Science* **377**, 670 (2022).
- [14] A. Cabot, F. Carollo, and I. Lesanovsky, Continuous sensing and parameter estimation with the boundary time crystal, *Phys. Rev. Lett.* **132**, 050801 (2024).
- [15] A. Auerbach, *Interacting Electrons and Quantum Magnetism*, 1994th ed. (Springer, New York, 1994).
- [16] J. Larson, B. Damski, G. Morigi, and M. Lewenstein, Mott-insulator states of ultracold atoms in optical resonators, *Phys. Rev. Lett.* **100**, 050401 (2008).
- [17] P. Kirton, M. M. Roses, J. Keeling, and E. G. D. Torre, Introduction to the Dicke model: From equilibrium to nonequilibrium, and vice versa, *Adv. Quantum Technol.* **2**, 1800043 (2019).
- [18] F. Mivehvar, F. Piazza, T. Donner, and H. Ritsch, Cavity QED with quantum gases: New paradigms in many-body physics, *Adv. Phys.* **70**, 1 (2021).
- [19] M. B. M. Svendsen and B. Olmos, Modified dipole-dipole interactions in the presence of a nanophotonic waveguide, *Quantum* **7**, 1091 (2023).
- [20] F. Le Kien and A. Rauschenbeutel, Nanofiber-mediated chiral radiative coupling between two atoms, *Phys. Rev. A* **95**, 023838 (2017).
- [21] B. Sbierski, M. Bintz, S. Chatterjee, M. Schuler, N. Y. Yao, and L. Pollet, Magnetism in the two-dimensional dipolar XY model, *Phys. Rev. B* **109**, 144411 (2024).
- [22] C. Chen, G. Bornet, M. Bintz, G. Emperauger, L. Leclerc, V. S. Liu, P. Scholl, D. Barredo, J. Hauschild, S. Chatterjee, M. Schuler, A. M. Läuchli, M. P. Zaletel, T. Lahaye, N. Y. Yao, and A. Browaeys, Continuous symmetry breaking in a two-dimensional Rydberg array, *Nature (London)* **616**, 691 (2023).
- [23] C. Chen, G. Emperauger, G. Bornet, F. Caleca, B. Gély, M. Bintz, S. Chatterjee, V. Liu, D. Barredo, N. Y. Yao, T. Lahaye, F. Mezzacapo, T. Roscilde, and A. Browaeys, Spectroscopy of elementary excitations from quench dynamics in a dipolar XY Rydberg simulator, [arXiv:2311.11726](https://arxiv.org/abs/2311.11726).
- [24] A. W. Sandvik, Computational studies of quantum spin systems, *AIP Conf. Proc.* **1297**, 135 (2010).

- [25] A. Lohmann, H.-J. Schmidt, and J. Richter, Tenth-order high-temperature expansion for the susceptibility and the specific heat of spin- s Heisenberg models with arbitrary exchange patterns: Application to pyrochlore and kagome magnets, *Phys. Rev. B* **89**, 014415 (2014).
- [26] P. Adelhardt, J. A. Koziol, A. Langheld, and K. P. Schmidt, Monte Carlo based techniques for quantum magnets with long-range interactions, *Entropy* **26**, 401 (2024).
- [27] H. Bruus, K. Flensberg, H. Bruus, and K. Flensberg, *Many-Body Quantum Theory in Condensed Matter Physics: An Introduction*, Oxford Graduate Texts (Oxford University Press, Oxford, 2004).
- [28] R. Agra, F. van Wijland, and E. Trizac, On the free energy within the mean-field approximation, *Eur. J. Phys.* **27**, 407 (2006).
- [29] R. Brout, Statistical mechanical theory of ferromagnetism. High density behavior, *Phys. Rev.* **118**, 1009 (1960).
- [30] W. Metzner and D. Vollhardt, Correlated lattice fermions in $d = \infty$, *Phys. Rev. Lett.* **62**, 324 (1989).
- [31] N. Defenu, T. Donner, T. Macri, G. Pagano, S. Ruffo, and A. Trombettoni, Long-range interacting quantum systems, *Rev. Mod. Phys.* **95**, 035002 (2023).
- [32] K. Hepp and E. H. Lieb, On the superradiant phase transition for molecules in a quantized radiation field: The dicke maser model, *Ann. Phys.* **76**, 360 (1973).
- [33] F. Carollo and I. Lesanovsky, Exactness of mean-field equations for open dicke models with an application to pattern retrieval dynamics, *Phys. Rev. Lett.* **126**, 230601 (2021).
- [34] H. Kleinert and V. Schulte-frohlinde, *Critical Properties of Phi-4-Theories*, 1st ed. (World Scientific, Singapore, 2001).
- [35] S. L. Sondhi, S. M. Girvin, J. P. Carini, and D. Shahar, Continuous quantum phase transitions, *Rev. Mod. Phys.* **69**, 315 (1997).
- [36] V. G. Vaks, A. I. Larkin, and S. A. Pikin, Self-consistent field method for the description of phase transitions, *Sov. Phys. JETP* **24**(1), 240 (1967).
- [37] V. G. Vaks and A. I. Larkin, Spin waves and correlation functions in a ferromagnetic, *Sov. Phys. JETP* **26**(3), 647 (1968).
- [38] R. B. Stinchcombe, Thermal and magnetic properties of the transverse Ising model, *J. Phys. C* **6**, 2507 (1973).
- [39] R. B. Stinchcombe, Ising model in a transverse field. I. Basic theory, *J. Phys. C* **6**, 2459 (1973).
- [40] R. B. Stinchcombe, Ising model in a transverse field. II. Spectral functions and damping, *J. Phys. C* **6**, 2484 (1973).
- [41] Y. A. Izumov and Y. N. Skryabin, *Statistical Mechanics of Magnetically Ordered Systems* (Consultants Bureau, New York, 1988).
- [42] J. Zhao, M. Song, Y. Qi, J. Rong, and Z. Y. Meng, Finite-temperature critical behaviors in 2D long-range quantum Heisenberg model, *npj Quantum Mater.* **8**, 59 (2023).
- [43] J. Gelhausen, M. Buchhold, A. Rosch, and P. Strack, Quantum-optical magnets with competing short- and long-range interactions: Rydberg-dressed spin lattice in an optical cavity, *SciPost Physics* **1**, 004 (2016).
- [44] A. Schellenberger and K. P. Schmidt, (Almost) everything is a Dicke model - Mapping non-superradiant correlated light-matter systems to the exactly solvable Dicke model, *SciPost Phys. Core* **7**, 038 (2024).
- [45] G. Horwitz and H. B. Callen, Diagrammatic expansion for the Ising model with arbitrary spin and range of interaction, *Phys. Rev.* **124**, 1757 (1961).
- [46] F. Englert, Linked cluster expansions in the statistical theory of ferromagnetism, *Phys. Rev.* **129**, 567 (1963).
- [47] R. Rossi, Determinant diagrammatic Monte Carlo in the thermodynamic limit, *Phys. Rev. Lett.* **119**, 045701 (2017).
- [48] R. Goll, D. Tarasevych, J. Krieg, and P. Kopietz, Spin functional renormalization group for quantum Heisenberg ferromagnets: Magnetization and magnon damping in two dimensions, *Phys. Rev. B* **100**, 174424 (2019).
- [49] J. Halbinger, B. Schneider, and B. Sbierski, Spectral representation of Matsubara n -point functions: Exact kernel functions and applications, *SciPost Phys.* **15**, 183 (2023).
- [50] J. Krieg and P. Kopietz, Exact renormalization group for quantum spin systems, *Phys. Rev. B* **99**, 060403(R) (2019).
- [51] J. Krieg, Doctoral thesis, Universitätsbibliothek Johann Christian Senckenberg, 2019, <https://publikationen.ub.uni-frankfurt.de/frontdoor/index/index/year/2020/docId/52628>.
- [52] A. M. Ferrenberg, J. Xu, and D. P. Landau, Pushing the limits of Monte Carlo simulations for the three-dimensional Ising model, *Phys. Rev. E* **97**, 043301 (2018).
- [53] P. H. Lundow and K. Markström, Critical behavior of the Ising model on the four-dimensional cubic lattice, *Phys. Rev. E* **80**, 031104 (2009).
- [54] P. Butera and M. Pernici, High-temperature expansions of the higher susceptibilities for the Ising model in general dimension d , *Phys. Rev. E* **86**, 011139 (2012).
- [55] J. Otsuki and Y. Kuramoto, Dynamical mean-field theory for quantum spin systems: Test of solutions for magnetically ordered states, *Phys. Rev. B* **88**, 024427 (2013).
- [56] S. McKenzie, C. Domb, and D. L. Hunter, The high-temperature susceptibility of the classical Heisenberg model in four dimensions, *J. Phys. A: Math. Gen.* **15**, 3909 (1982).
- [57] J. Oitmaa and W. Zheng, Curie and Néel temperatures of quantum magnets, *J. Phys.: Condens. Matter* **16**, 8653 (2004).
- [58] H. W. J. Blöte and Y. Deng, Cluster Monte Carlo simulation of the transverse Ising model, *Phys. Rev. E* **66**, 066110 (2002).
- [59] I. V. Lukin, A. G. Sotnikov, J. M. Leamer, A. B. Magann, and D. I. Bondar, Spectral gaps of two- and three-dimensional many-body quantum systems in the thermodynamic limit, *Phys. Rev. Res.* **6**, 023128 (2024).
- [60] N. D. Mermin and H. Wagner, Absence of ferromagnetism or antiferromagnetism in one- or two-dimensional isotropic Heisenberg models, *Phys. Rev. Lett.* **17**, 1133 (1966).
- [61] Y. Zhang, L. Yu, J.-Q. Liang, G. Chen, S. Jia, and F. Nori, Quantum phases in circuit QED with a superconducting qubit array, *Sci. Rep.* **4**, 4083 (2014).
- [62] J. Rohn, M. Hörmann, C. Genes, and K. P. Schmidt, Ising model in a light-induced quantized transverse field, *Phys. Rev. Res.* **2**, 023131 (2020).
- [63] G. Pupillo, A. Micheli, M. Boninsegni, I. Lesanovsky, and P. Zoller, Strongly correlated gases of rydberg-dressed atoms: Quantum and classical dynamics, *Phys. Rev. Lett.* **104**, 223002 (2010).
- [64] M. Weber, Quantum Monte Carlo simulation of spin-boson models using wormhole updates, *Phys. Rev. B* **105**, 165129 (2022).
- [65] E. G. D. Torre, S. Diehl, M. D. Lukin, S. Sachdev, and P. Strack, Keldysh approach for nonequilibrium phase transitions

- in quantum optics: Beyond the Dicke model in optical cavities, *Phys. Rev. A* **87**, 023831 (2013).
- [66] D. Peter, S. Müller, S. Wessel, and H. P. Büchler, Anomalous behavior of spin systems with dipolar interactions, *Phys. Rev. Lett.* **109**, 025303 (2012).
- [67] M. A. Cazalilla and A. M. Rey, Ultracold Fermi gases with emergent SU(N) symmetry, *Rep. Prog. Phys.* **77**, 124401 (2014).
- [68] X. Zhang, M. Bishof, S. L. Bromley, C. V. Kraus, M. S. Safronova, P. Zoller, A. M. Rey, and J. Ye, Spectroscopic observation of SU(N)-symmetric interactions in Sr orbital magnetism, *Science* **345**, 1467 (2014).
- [69] Yu. A. Izyumov, N. I. Chaschin, and V. Yu. Yushankhai, Longitudinal spin dynamics in the Heisenberg ferromagnet: Diagrammatic approach, *Phys. Rev. B* **65**, 214425 (2002).
- [70] T. Chen, A. Ghasemi, J. Zhang, L. Shi, Z. Tagay, L. Chen, E.-S. Choi, M. Jaime, M. Lee, Y. Hao, H. Cao, B. Winn, R. Zhong, X. Xu, N. P. Armitage, R. Cava, and C. Broholm, Phase diagram and spectroscopic evidence of supersolids in quantum Ising magnet $K_2Co(SeO_3)_2$, [arXiv:2402.15869](https://arxiv.org/abs/2402.15869).
- [71] B. Schneider and B. Sbierski, Taming spin susceptibilities in frustrated quantum magnets: Mean-field form and approximate nature of the quantum-to-classical correspondence, [arXiv:2407.09401](https://arxiv.org/abs/2407.09401).
- [72] S. A. Kulagin, N. Prokof'ev, O. A. Starykh, B. Svistunov, and C. N. Varney, Bold diagrammatic Monte Carlo method applied to fermionized frustrated spins, *Phys. Rev. Lett.* **110**, 070601 (2013).
- [73] R. Burkard *et al.* (unpublished).
- [74] A. Rückriegel, D. Tarasevych, J. Krieg, and P. Kopietz, Recursive algorithm for generating high-temperature expansions for spin systems and the chiral nonlinear susceptibility, *Phys. Rev. B* **110**, 144416 (2024).
- [75] F. B. Kugler, S.-S. B. Lee, and J. von Delft, Multipoint correlation functions: Spectral representation and numerical evaluation, *Phys. Rev. X* **11**, 041006 (2021).